## ONLINE METHODS

**Subjects.** We studied 92 children (61 boys and 31 girls) with JMML, including 7 individuals with NS/MPD, who were diagnosed as having JMML in institutions throughout Japan. Written informed consent was obtained from subjects' parents before sample collection. This study was approved by the ethics committees of the Nagoya University Graduate School of Medicine and the University of Tokyo in accordance with the Declaration of Helsinki. Diagnosis with JMML was made on the basis of internationally accepted criteria[1]. Characteristics of the 92 JMML cases are summarized in **Table 2**. The median age at diagnosis was 16 months (range of 1–160 months). Karyotypic abnormalities were detected in 16 subjects, including in 8 with monosomy 7. Fifty-six of the 92 subjects (61%) received allogeneic HSCT.

**Sample preparation.** Genomic DNA was extracted using the QIAamp DNA Blood Mini kit and the QIAamp DNA Investigator kit (Qiagen) according to the manufacturer's instructions. The T Cell Activation/Expansion kit, human (Miltenyi Biotec) was used for the expansion of $CD3^+$ T cells from subjects' peripheral blood or bone marrow mononuclear cells[3].

**Whole-exome sequencing.** Exome capture from paired tumor-reference DNA was performed using SureSelect Human All Exon V3 (Agilent Technologies), covering 50 Mb of coding exons, according to the manufacturer's protocol. Enriched exome fragments were subjected to massively parallel sequencing using the HiSeq 2000 platform (Illumina). Candidate somatic mutations were detected through our in-house pipeline (Genomon) as previously described[17].

**Detection of mutations from whole-exome sequencing data.** Detection of candidate somatic mutations was performed according to previously described algorithms with minor modifications[17]. Briefly, the number of reads containing single-nucleotide variations (SNVs) and indels in both tumor and reference samples was determined using SAMtools[31], and the null hypothesis of equal allele frequencies in tumor and reference samples was tested using the two-tailed Fisher's exact test. A variant was adopted as a candidate somatic mutation if it had $P < 0.01$, if it was observed in bidirectional reads (in both plus and minus strands of the reference sequence) and if its allele frequency was less than 0.25 in the corresponding reference sample. For the detection of germline mutations in RAS pathway genes, SNVs and indels having allele frequencies of more than 0.25 (SNVs) and 0.10 (indels) were interrogated for 46 genes, which consisted of known JMML-related RAS pathway genes and genes registered in the pathway databases ('Ras signaling pathway' in BioCarta and 'signaling to RAS' in Reactome[32]). For variant calls in tumor samples for which the paired normal reference was not available, candidate variants in the RAS pathway were detected at an allele frequency of >0.10. Finally, the list of candidate somatic and/or germline mutations was generated by excluding synonymous SNVs and other variants registered in either dbSNP131 or an in-house SNP database constructed from 180 individual samples. All candidates were validated by Sanger sequencing as previously described.

**Estimation of tumor content.** The tumor content of bone marrow specimens was estimated from the allele frequency of the somatic mutations identified by deep sequencing. For homozygous mutations, as indicated by an allele frequency of >0.75, the tumor content ($F_{tumor}$) was calculated from the observed frequency ($F_{observed}$) of the mutation according to the following equation: $F_{tumor} = 2 \times F_{observed} - 1$. For heterozygous mutations, the tumor content was calculated by doubling the allele frequency.

**Power analysis of whole-exome sequencing.** The power of detecting somatic mutations at each nucleotide position in whole-exome sequencing was estimated by Monte-Carlo simulation ($n$ = 1,000) on the basis of the observed mean depth of coverage for each exon in germline and tumor samples and the observed tumor content for each sample, which were estimated using the allele frequencies of the observed mutations. For the samples with no observed somatic mutations, the average tumor content of the informative samples was employed. Simulations were performed across a total of 192,424 exons.

**Copy number analysis in whole-exome sequencing data.** To detect copy number lesions at a single-exon level, the mean coverage of each exon normalized by the mean depth of coverage of the entire sample was compared with that of 12 unrelated normal DNA samples. Exons showing normalized coverage greater than 3 s.d. from the mean coverage of the reference samples were called as candidates for copy number alterations. All candidate exons of RAS pathway genes were visually inspected using the Integrative Genomics Viewer[33] and were validated by Sanger sequencing of corresponding putative breakpoint-containing fragments.

**Targeted deep sequencing.** Deep sequencing of the targeted genes was performed essentially as described in the 'deep sequencing of pooled target exons' section in ref. 17, except that target DNA was not pooled. Briefly, all exons of *PTPN11*, *NF1*, *KRAS*, *NRAS*, *CBL*, *SETBP1*, *JAK3* and *SH3BP1* were PCR amplified with Quick Taq HS DyeMix (TOYOBO) and the PrimeSTAR GXL DNA Polymerase kit (Takara Bio) using primers including the NotI restriction site (**Supplementary Table 3**). The PCR products from an individual sample were combined and purified with the QIAquick PCR Purification kit (Qiagen) for subsequent digestion with NotI (Fermentas). Digested PCR product was purified, concatenated with T4 DNA ligase (Takara Bio) and sonicated to generate fragments with an average size of 150 bp using Covaris. Fragments were processed for sequencing according to a modified Illumina paired-end library protocol, and sequences were read by a HiSeq 2000 instrument using a 100-bp paired-end read protocol.

**Variant calls in targeted deep sequencing.** Data processing and variant calling were performed with modifications to the protocol described in a previous publication[17]. Each read was aligned to the set of targeted sequences from PCR amplification, with BLAT[34] instead of Burrows-Wheeler Aligner (BWA)[35] used with the -fine option. Mapping information in the .psl format was converted to the .sam format with paired-read information. Of the successfully mapped reads, reads were excluded from further analysis if they mapped to multiple sites, mapped with more than four mismatched bases or had more than ten soft-clipped bases. Next, the Estimation_CRME script was run to eliminate strand-specific errors and exclude PCR-derived errors. A strand-specific mismatch ratio was calculated for each nucleotide variant for both strands using the bases from read cycles 11 to 50 on the next-generation sequencer. By excluding the top five cycles showing the highest mismatch rates, strand-specific mismatch rates were recalculated, and the smaller value between both strands was adopted as a nominal mismatch ratio for that variant. After excluding variants found in dbSNP131 or the in-house SNP database, non-silent variants having a mismatch ratio of greater than 0.05 were called as candidates, unless they had median values of the mismatch ratio at the relevant nucleotide positions in the 92 samples of greater than 0.01, as such variants were likely to be caused by systematic PCR problems. Finally, candidates with mismatch ratios of >0.15 were further validated by Sanger sequencing.

**Annotation of the detected mutations.** Detected mutations were annotated using ANNOVAR[36]. The positions of the mutations were based on the following RefSeq transcript sequences: NM_002834.3 for *PTPN11*, NM_000267.3 for *NF1*, NM_002524.4 for *NRAS*, NM_004985.3 for *KRAS*, NM_005188.3 for *CBL*, NM_015559.2 for *SETBP1* and NM_000215.3 for *JAK3*. The effect of the mutations on protein function was assessed by SIFT[37], PolyPhen-2 (ref. 38) and MutationTaster[39].

**Whole-genome sequencing.** Paired tumor-reference DNA samples were sequenced with the HiSeq 2000 platform according to the manufacturer's instructions to obtain 30× read coverage for reference samples and 40× coverage for tumor samples. Obtained FASTQ sequences were aligned to the human reference genome (hg19) using BWA[35] 0.5.8 with default parameters. Alignment of pairs of sequences, at least one of which was not mapped or was considered to have possible mapping problems (with mapping quality of less than 40, insertions or deletions, soft-clipped sequence of more than 10% of the length of the original sequence, irregular paired-read orientation or mate distance of greater than 2,000 bp), was attempted with BLAT[34] using default parameters, except for stepSize = 5 and repMatch = 2,253. Mapping statistics were calculated by counting the bases at each genomic position with SAMtools[31]. For variant calling, variant and reference bases with base quality of >30 were counted in both germline and tumor samples, and the Fisher's

exact test was applied. Variants with $P$ of <0.01 were called. Variants having allele frequency of >0.25 in the germline sample were excluded. Variants found in 12 unrelated germline samples with an allele frequency of >0.01 on average were also excluded owing to the high probability that they represented false positive calls. Copy number estimation was performed by calculating the averaged ratio of read depths in germline and tumor samples in 10,000-base bins. An allele-specific copy number plot was generated by measuring the allele frequency of the tumor sample at the positions in which more than 25% of the allele mismatch was observed in germline samples. For the detection of chromosomal structural variations, soft-clipped sequences that could be mapped to a unique genomic position were selected. Structural variation candidates that had more than four supporting read pairs in total and at least one read pair from each side of the breakpoint were called. Contig sequences were generated by assembling the reads within 200 bp of the breakpoint with CAP3 (ref. 40), and structural variations having the contig sequence that could be aligned to the alternate assembly of the hg19 genome with more than 93% identity were excluded as false positives. Structural variations with read depth of greater than 150 on at least one side of the breakpoint were considered to be mapped to a repeat element and were also excluded. For detection of viruses, unmapped sequences were aligned to the collection of all viral genomes in the RefSeq database using BLAT. A virus was considered to be detected if its genome was covered by mean read coverage of >1.

**cDNA sequencing.** Total RNA was extracted using the RNeasy Mini kit (Qiagen) and was reverse transcribed with the ThermoScript RT-PCR system (Life Technologies). Target sequences were PCR amplified with the PrimeSTAR GXL DNA Polymerase kit using the primers listed in **Supplementary Table 3** and were sequenced.

**Statistical analysis.** For comparison of the frequency of mutations or other clinical features between disease groups, categorical variables were analyzed using the Fisher's exact test, and continuous variables were tested using the Mann-Whitney $U$ test. Overall survival and transplantation-free survival were estimated by the Kaplan-Meier method. Hazard ratios for survival with 95% CIs were estimated according to the Cox proportional hazards model, and difference in survival was tested by log-rank test. STATA version 12.0 (StataCorp) was used for all statistical calculations.


31. Li, H. *et al.* The Sequence Alignment/Map format and SAMtools. *Bioinformatics* **25**, 2078–2079 (2009).
32. Matthews, L. *et al.* Reactome knowledgebase of human biological pathways and processes. *Nucleic Acids Res.* **37**, D619–D622 (2009).
33. Thorvaldsdóttir, H., Robinson, J.T. & Mesirov, J.P. Integrative Genomics Viewer (IGV): high-performance genomics data visualization and exploration. *Brief. Bioinform.* **14**, 178–192 (2013).
34. Kent, W.J. BLAT—the BLAST-like alignment tool. *Genome Res.* **12**, 656–664 (2002).
35. Li, H. & Durbin, R. Fast and accurate short read alignment with Burrows-Wheeler transform. *Bioinformatics* **25**, 1754–1760 (2009).
36. Wang, K., Li, M. & Hakonarson, H. ANNOVAR: functional annotation of genetic variants from high-throughput sequencing data. *Nucleic Acids Res.* **38**, e164 (2010).
37. Kumar, P., Henikoff, S. & Ng, P.C. Predicting the effects of coding non-synonymous variants on protein function using the SIFT algorithm. *Nat. Protoc.* **4**, 1073–1081 (2009).
38. Adzhubei, I.A. *et al.* A method and server for predicting damaging missense mutations. *Nat. Methods* **7**, 248–249 (2010).
39. Schwarz, J.M., Rödelsperger, C., Schuelke, M. & Seelow, D. MutationTaster evaluates disease-causing potential of sequence alterations. *Nat. Methods* **7**, 575–576 (2010).
40. Huang, X. & Madan, A. CAP3: A DNA sequence assembly program. *Genome Res.* **9**, 868–877 (1999).

Rheumatology Advance Access published December 3, 2013
RHEUMATOLOGY


Original article

doi:10.1093/rheumatology/ket372

# A nationwide survey of Aicardi-Goutières syndrome patients identifies a strong association between dominant *TREX1* mutations and chilblain lesions: Japanese cohort study

**Junya Abe[1], Kazuyuki Nakamura[2], Ryuta Nishikomori[1], Mitsuhiro Kato[2], Noriko Mitsuiki[3,4], Kazushi Izawa[1], Tomonari Awaya[1], Tomoki Kawai[1], Takahiro Yasumi[1], Itaru Toyoshima[5], Kazuko Hasegawa[6], Yusei Ohshima[7], Toru Hiragi[8], Yoji Sasahara[9], Yasuhiro Suzuki[10], Masahiro Kikuchi[11], Hitoshi Osaka[12], Takashi Ohya[13], Shinya Ninomiya[14], Satoshi Fujikawa[15], Manami Akasaka[16], Naomi Iwata[17], Akiko Kawakita[7], Makoto Funatsuka[18], Haruo Shintaku[19], Osamu Ohara[3,20], Hiroshi Ichinose[21] and Toshio Heike[1]**

## Abstract

**Objectives.** Aicardi-Goutières syndrome (AGS) is a rare, genetically determined, early onset progressive encephalopathy associated with autoimmune manifestations. AGS is usually inherited in an autosomal recessive manner. The disease is rare, therefore the clinical manifestations and genotype–phenotype correlations, particularly with regard to autoimmune diseases, are still unclear. Here we performed a nationwide survey of AGS patients in Japan and analysed the genetic and clinical data.

**Methods.** Patients were recruited via questionnaires sent to paediatric or adult neurologists in Japanese hospitals and institutions. Genetic analysis was performed and clinical data were collected.

**Results.** Fourteen AGS patients were identified from 13 families; 10 harboured genetic mutations. Three patients harboured dominant-type *TREX1* mutations. These included two *de novo* cases: one caused by a novel heterozygous p.His195Tyr mutation and the other by a novel somatic mosaicism resulting in a p.Asp200Asn mutation. Chilblain lesions were observed in all patients harbouring dominant-type *TREX1* mutations. All three patients harbouring *SAMHD1* mutations were diagnosed with autoimmune diseases, two with SLE and one with SS. The latter is the first reported case.

**Conclusion.** This study is the first to report a nationwide AGS survey, which identified more patients with sporadic AGS carrying *de novo* dominant-type *TREX1* mutations than expected. There was a strong association between the dominant-type *TREX1* mutations and chilblain lesions, and between *SAMHD1* mutations and autoimmunity. These findings suggest that rheumatologists should pay attention to possible sporadic AGS cases presenting with neurological disorders and autoimmune manifestations.

**Key words:** Aicardi-Goutières syndrome, *TREX1*, *SAMHD1*, dominant-type, mosaicism, chilblain, autoimmunity.

[1]Department of Pediatrics, Kyoto University Graduate School of Medicine, Kyoto, [2]Department of Pediatrics, Yamagata University Faculty of Medicine, Yamagata, [3]Department of Human Genome Research, Kazusa DNA Research Institute, Kisarazu, [4]Department of Pediatrics and Developmental Biology, Graduate School of Medical and Dental Sciences, Tokyo Medical and Dental University, Tokyo, [5]Department of Neurology, National Hospital Organization Akita National Hospital, Yurihonjo, [6]Department of Neurology, National Hospital Organization, Sagamihara National Hospital, Sagamihara, [7]Department of Pediatrics, Faculty of Medical Sciences, University of Fukui, Fukui, [8]Department of Pediatrics, Tsuruga Municipal Hospital, Tsuruga, [9]Department of Pediatrics, Tohoku University Graduate School of Medicine, Sendai, [10]Department of Pediatric Neurology, Osaka Medical Center and Research Institute for Maternal and Child Health, Izumi, [11]Department of Pediatrics, Hitachi General Hospital, Hitachi, [12]Department of Neurology, Kanagawa Children's Medical Center, Yokohama, [13]Department of Pediatrics and Child Health, Kurume University School of Medicine, Kurume, [14]Department of Pediatrics, Nakatsu Municipal Hospital, Nakatsu, [15]Fujikawa Pediatrics Clinic, Tokyo, [16]Department of Pediatrics, Iwate Medical University School of Medicine, Morioka, [17]Department of Infection and Immunology, Aichi Children's Health and Medical Center, Obu, [18]Department of Pediatrics, Tokyo Women's Medical University, Tokyo, [19]Department of Pediatrics, Osaka City University Graduate School of Medicine, Osaka, [20]Laboratory for Immunogenomics, RIKEN Research Center for Allergy and Immunology, RIKEN Yokohama Institute, Yokohama and [21]Department of Life Science, Graduate School of Bioscience and Biotechnology, Tokyo Institute of Technology, Yokohama, Japan.

Submitted 22 July 2013; revised version accepted 24 September 2013.

Correspondence to: Ryuta Nishikomori, Department of Pediatrics, Kyoto University Graduate School of Medicine, 54 Kawahara-cho, Shogoin, Sakyo-ku, Kyoto 606-8507, Japan. E-mail: rnishiko@kuhp.kyoto-u.ac.jp

## Introduction

Aicardi-Goutières syndrome (AGS) is a rare, genetically determined, early onset progressive encephalopathy [1]. Patients with AGS typically suffer from irritability, inconsolable crying and progressive microcephaly associated with severe neurological symptoms, such as hypotonia, dystonia, seizures, spastic quadriplegia and severe developmental delay [2]. On brain imaging, AGS is characterized by calcifications of basal ganglia, white matter abnormalities and cerebral atrophy [3, 4]. Cerebrospinal fluid (CSF) analysis shows chronic lymphocytosis and elevated IFN-α and neopterin levels [3–5]. AGS patients are often misdiagnosed as having intrauterine infections, such as TORCH (toxoplasmosis, other infections, rubella, cytomegalovirus infection and herpes simplex) syndrome, because of the similarities in the clinical findings, particularly the intracranial calcifications [1]. As extraneural findings, chilblain lesions are seen in approximately 40% of patients [3]. Some patients also show bouts of mild fever, hepatosplenomegaly, abnormal liver function and thrombocytopenia [1, 3, 4].

Mutations in five genes—*TREX1*, *RNASEH2B*, *RNASEH2C*, *RNASEH2A* and *SAMHD1*—are linked with AGS [6–8]. Approximately 90% of patients with characteristic clinical and radiologic findings of AGS harbour aetiological mutations in one of these five genes [1]. The *ADAR1* gene was recently identified as a sixth gene linked with AGS [9]. AGS is often inherited in an autosomal recessive manner, although a few cases show an autosomal dominant pattern of inheritance [2, 10–12]. Mutations in *TREX1* are often associated with early onset neonatal AGS, which presents with more severe neurological features, whereas *RNASEH2B* mutations are related to a later-onset presentation that is associated with less severe neurological problems and lower mortality rates [2, 3].

The main pathophysiological feature of AGS is the overproduction of type I IFN, caused by the accumulation of nucleic acids within cells stimulating the pattern recognition receptors and the innate immune system [1]. Therefore AGS can be regarded as an interferonopathy [13]. SLE is also an interferonopathy and shares many clinical features with AGS, including skin lesions, neurological abnormalities and the expression of type I IFN-related genes [13, 14]. Some SLE patients harbour *TREX1* mutations, suggesting that AGS and SLE are both allelic disorders that share a common pathophysiology, overproduction of type I IFN [15]. AGS is a disease of monogenic autoimmunity and an important disorder that must be considered when making a differential diagnosis of SLE; indeed, some molecularly proven AGS patients fulfil the diagnostic criteria for SLE [2, 16, 17]. In addition, AGS is similar, particularly with regard to skin lesions, to familial chilblain lupus (FCL), a rare cutaneous form of SLE that shows Mendelian inheritance [18]. We recently reported a family containing AGS and FCL cases caused by a heterozygous p.Asp18Asn mutation in *TREX1*, and proved the clinical continuity of these two conditions [19]. Although the similarities between SLE and AGS are known, the autoimmune aspects of AGS are still unclear because of the rarity of the disorder.

As a rare monogenic disorder, AGS reports have predominantly examined individual AGS families. Alternatively, some genetic analysis centres have recruited AGS patients from around the world. Here we report the first nationwide survey of Japanese AGS patients, which was conducted using questionnaires designed to identify the clinical manifestations and genotype–phenotype correlations in detail, with a particular focus on autoimmune symptoms.

## Materials and methods

### Patients

Questionnaires were sent to 1852 hospitals and institutions that specialize in paediatric and adult neurology, and 760 replies (41.0%) were received. Detailed questionnaires were then sent to the hospitals or institutions with positive replies and clinical information regarding suspected AGS cases was obtained. In addition, some patients enrolled in the study were referred directly to our institution by paediatric neurologists and paediatric rheumatologists. Clinical information, patient histories and laboratory data were collected from medical records and by direct interviews with patients, their families and their attending physicians. Neuroimaging data included CT scans and/or MRI scans. AGS was diagnosed according to the following criteria: (i) neurological abnormalities of encephalopathy, (ii) intracranial calcifications, (iii) the absence of prenatal infection and (iv) at least one CSF abnormality, such as a white cell count $\geqslant 5$ cells/mm$^3$, elevated IFN-α levels (>6 IU/ml or >12.5 pg/ml), or raised neopterin levels (reference ranges 8.0–25.0 nM at an age of 2–12 years and 7.3–31.6 nM in adults). In cases with no available CSF data, a diagnosis of AGS was made when the patients fulfilled criteria 1–3 and either had mutations in the genes responsible for AGS or had siblings who had been diagnosed with AGS.

### Laboratory data

IFN-α levels were measured using a cytopathic effect inhibition assay (SRL, Tokyo, Japan). In the present study, a value >6 IU/ml was considered elevated due to the limit of detection of the assay, although most previous reports considered >2 IU/ml as the cut-off value for AGS. In some cases, IFN-α was measured by ELISA (SRL). The CSF neopterin level was measured as previously described [20].

### Genetic analysis

The nationwide survey was approved by the ethical committee of the National Hospital Organization, Sagamihara National Hospital, and genetic analyses were approved by the ethical committees of Kyoto University Hospital and the National Hospital Organization, Sagamihara National Hospital, in accordance with the Declaration of Helsinki. After obtaining written informed consent from all study subjects (or their parents or guardians), genetic analyses

of *TREX1*, *RNASEH2B*, *RNASEH2C*, *RNASEH2A* and *SAMHD1* were performed. Genetic analysis of the *ADAR1* gene was performed for those patients clinically diagnosed with AGS but who did not harbour a mutation in any of these genes. Genomic DNA was extracted from the whole blood samples taken from the patients and their parents (if available) and all exons, including the exon–intron boundaries, were sequenced as previously described [21]. *TREX1* gene mosaicism was analysed using massively parallel DNA sequencing as previously described [22]. Leucocyte subpopulations were isolated and sorted using an autoMACS Pro Separator (Miltenyi Biotec, Gladbach, Germany) as previously described [23]. The purity of the isolated subpopulations was >90%.

### Exonuclease assays

The pFN18A HaloTag T7 Flexi Vector system (Promega, Madison, WI, USA) with a HaloTag at the N-terminus was used to generate a recombinant human TREX1 protein. Recombinant protein was produced in Single Step (KRX) Competent Cells (Promega) and isolated according to the manufacturer's protocol. The recombinant proteins were then immunoblotted with an anti-TREX1 antibody (Sigma-Aldrich, St Louis, MO, USA) as previously described [21]. The concentrations of the purified TREX1 proteins were determined using the Flamingo Fluorescent Gel Stain (Bio-Rad, Hercules, CA, USA) assay with a Molecular Imager FX Pro Plus (Bio-Rad).

The ssDNA and dsDNA exonuclease assays were performed according to the method of Orebaugh *et al.* [24]. Briefly, for the ssDNA assays, a 30-mer oligonucleotide with 5′-fluorescein (6-FAM) (Sigma-Aldrich) and TREX1 proteins were incubated at 37°C for 30 min, followed by separation on 23% denaturing polyacrylamide gels. Using the visualized fluorescein-labelled bands, the fraction of oligomer at each position was multiplied by the number of excised deoxynucleoside monophosphates (dNMPs) to determine the activities of the recombinant TREX1 proteins (fmol of dNMP/s/fmol of enzyme). For the dsDNA assays, the p3xFLAG CMV-14 plasmid (Sigma-Aldrich), which contains a single Nt.BbvCI site (New England Biolabs, Ipswich, MA, USA), was digested by Nt.BbvCI. The nicked plasmid DNA was then incubated with the TREX1 proteins at 25°C for 30 min, followed by separation in electrophoresis on 0.8% agarose gels. Using SYBR Green I (Lonza, Basel, Switzerland), the excised dNMPs and activities of the recombinant TREX1 proteins (fmol of dNMP/s/fmol of enzyme) were calculated by the amount of degraded dsDNA.

### Statistical analysis

Fisher's exact test was used to examine differences in categorical variables among the cohort in the present study or between the cohort in the present study and cohorts from other studies. Statistical significance was set at $P < 0.05$.

## Results

### Genetic and molecular findings

We identified 14 AGS patients from 13 families. All patients were Japanese and none were consanguineous. Of the 13 families, 10 harboured mutations and 3 did not (Table 1). Altogether, we identified 15 mutations in four genes, 10 of which were novel. All of the novel mutations were absent from at least 100 Japanese control alleles and from the 1000 Genomes Project database. Six of the novel mutations were missense mutations. PolyPhen-2 analysis predicted five to be probably damaging and the other, a p.Gly258Val mutation in *SAMHD1*, to be possibly damaging; all were predicted to be deleterious by sorting intolerant from tolerant (SIFT) analysis. The median age of the patients at the time of genetic analysis was 6 years (range 6 months–18 years).

Of the 10 families harbouring mutations, 5 harboured mutations in *TREX1*, 3 in *SAMHD1*, 1 in *RNASEH2B* and 1 in *RNASEH2A*. None of the families harboured mutations in *RNASEH2C* or *ADAR1*. No families harboured homozygous mutations. The *RNASEH2B* mutation was heterozygous; however, the mother who showed no symptoms of AGS shared the same heterozygous

TABLE 1 Genetic findings of Aicardi-Goutières syndrome patients

| Patient | Gene | Nucleotide change | Protein change |
|---|---|---|---|
| 1 | AGS1/*TREX1* | c.[52G>A];[=] | p.[Asp18Asn];[=] |
| 2 | AGS1/*TREX1* | c.[**583C>T**];[=], *de novo* | p.[**His195Tyr**];[=], *de novo* |
| 3 | AGS1/*TREX1* | c.[=/598G>A], *de novo* | p.[=/Asp200Asn], *de novo* |
| 4 | AGS1/*TREX1* | c.[**667G>A**];[**839delG**] | p.[**Ala223Thr**];[**Gly280Glufs*18**] |
| 5 | AGS1/*TREX1* | c.[**839delG**];[859_876del18] | p.[**Gly280Glufs*18**];[Leu287_Gly292del] |
| 6 | AGS2/*RNASEH2B* | c.[**155T>G**];[=] | p.[**Leu52Trp**];[=] |
| 7 | AGS4/*RNASEH2A* | c.[**557G>A**];[**703C>T**] | p.[**Arg186Gln**];[**Arg235Trp**] |
| 8 | AGS5/*SAMHD1* | c.[368A>C];[**1567A>T**] | p.[His123Pro];[**Lys523***] |
| 9 | AGS5/*SAMHD1* | c.[**773G>T**];[**1141_1143delATT**] | p.[**Gly258Val**];[**Ile381del**] |
| 10 | AGS5/*SAMHD1* | c.[428G>A(;)**1435G>T**] | p.[Arg143His(;)**Glu479***] |

Novel mutations are indicated in bold. Consanguinity was not present in any of the families of these AGS patients. = denotes normal sequence, and * denotes nonsense variant.

mutation and further analyses were not performed due to a lack of additional samples of the patient or the family.

Three families (patients 1-3) harboured *TREX1* mutations on one allele only. The patient harbouring the heterozygous p.Asp18Asn mutation (patient 1) had a maternal family history of FCL, which was caused by the same mutation [19]. Parental genotyping showed that the other two mutations, p.His195Tyr and p.Asp200Asn (patients 2 and 3), were *de novo* (Fig. 1A and B). RT-PCR analyses also confirmed a lack of additional mutations in *TREX1* of the three patients.

Since dominant-type *TREX1* mutations are a very rare cause of AGS [2, 10-12], we performed additional biochemical analyses of the three dominant mutations identified in our cohort, particularly the novel p.His195Tyr mutation (patient 2), to confirm their mutational effects. The TREX1 protein contains three exonuclease domains that form the active site of the enzyme, and His195, located in the third exonuclease domain, is the catalytically important histidine (Fig. 1C) [25-28]. First, we confirmed that His195 was highly conserved among different species (Fig. 1D). Next, we generated recombinant human TREX1 proteins (Fig. 1E) and compared them with wild-type TREX1 proteins ($TREX1^{WT}$). The ssDNA and dsDNA exonuclease assays revealed that TREX1 proteins harbouring the p.His195Tyr mutation ($TREX1^{p.His195Tyr}$) showed a marked reduction in enzymatic activity, similar to TREX1 proteins harbouring the p.Asp18Asn ($TREX1^{p.Asp18Asn}$) and p.Asp200Asn ($TREX1^{p.Asp200Asn}$) mutations, which are reported to cause dominant-type AGS (Fig. 1F and G) [10, 11].

In addition, we identified a patient harbouring *TREX1* with a p.Asp200Asn mutation (patient 3), in which the signal intensity of the mutated A at position 598 was lower than that of the reference G (Fig. 1B). Since this result suggested that a somatic mosaicism can cause AGS, we performed additional genetic analyses. Massively parallel DNA sequencing showed that neutrophils, monocytes, T cells, B cells and cells of the buccal mucosa harboured the same mutation at frequencies of approximately 20-30%, suggesting that the mutation occurred at an early stage of development and that approximately half of the mutated and normal cells co-existed in the patient.

Fig. 1 Genetic and molecular analyses of the *TREX1* mutations

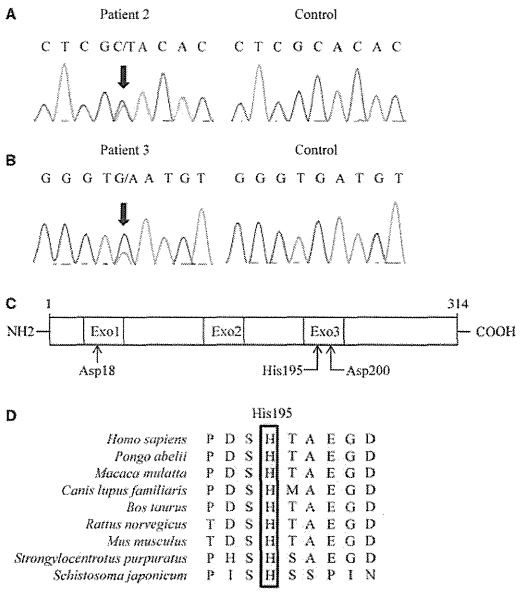


(**A**) Chromatograms for the direct sequencing of the *TREX1* gene from patient 2 and from a healthy control. The arrow indicates the heterozygous c.583C>T substitution, which leads to the p.His195Tyr mutation. (**B**) Chromatograms for the direct sequencing of the *TREX1* gene from patient 3 and from a healthy control. The arrow indicates the mutant A allele: the signal intensity of this mutation, at position 598, is lower than that of the reference G, suggesting somatic mosaicism of c.598G>A, which leads to the p.Asp200Asn mutation. (**C**) Schematic representation of the human TREX1 protein. Exo1-3 shows the three exonuclease domains that form the active site. The arrows indicate the positions of Asp18, His195 and Asp200. Mutations in these amino acid residues can cause dominantly inherited AGS. (**D**) Alignment of the TREX1 protein sequences. His195 is highly conserved from *Schistosoma japonicum* to *Homo sapiens*.

## Clinical findings

All of the patients in the present cohort are currently alive (Table 2). Of the 13 patients for whom neonatal information was available, 11 were born at term, but 6 were small for their gestational age. All patients showed the first symptoms of AGS within 6 months of birth, with a median disease onset of 1.5 months. Four patients (patients 9, 11, 13 and 14) were early onset cases, which were affected within the first days of life; patients 9 and 11 had thrombocytopenia at the time of disease onset. Of the other subacute-onset cases, the earliest symptoms were largely related to encephalopathy, including neurological abnormalities and fever; however, patients 1 and 2 presented with rashes on the extremities that were later diagnosed as chilblains.

In the present study, all patients showed developmental delay, which was severe in 13 cases and moderate in 1 (patient 1). Seizures were observed in seven patients (patients 1, 5, 7, 8, 11, 13 and 14), including febrile convulsions in two. We also identified microcephaly in nine patients (patients 4-10, 12 and 14), dystonia in six (patients 5, 6, 8, 9, 12 and 13) and hypotonia in five (patients 2, 5, 7, 9 and 13).

Chilblain lesions were observed in seven patients (patients 1-5, 8 and 10) (Fig. 2A). All five patients harbouring *TREX1* mutations had chilblain lesions, which were absent in patients without gene mutations. The lesions

FIG. 2 Genetic and molecular analysis of the *TREX1* mutations

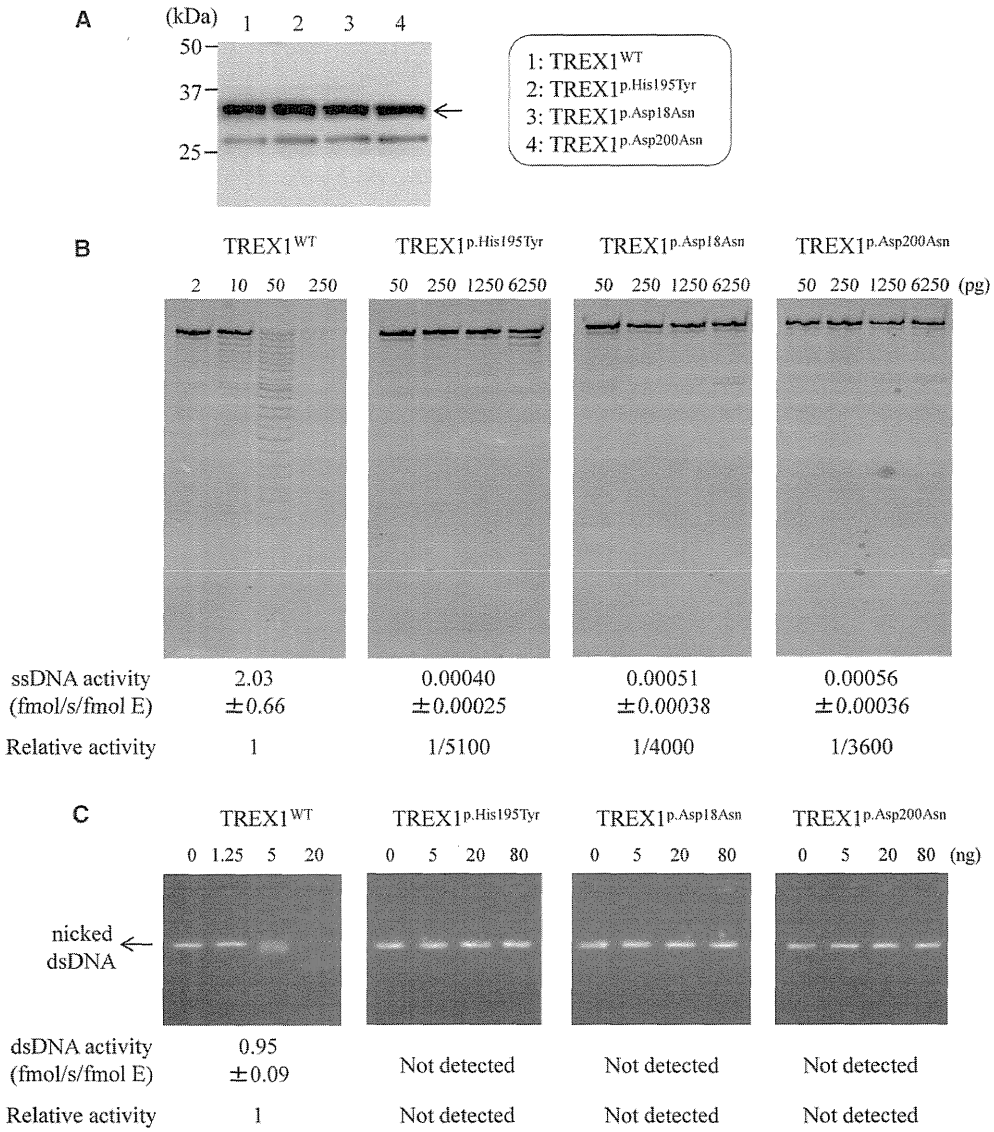


(**A**) Western blotting of purified recombinant human TREX1 proteins expressed in bacteria. The arrow indicates the position of the TREX1 proteins. The exonuclease activity of the recombinant TREX1 proteins in the (**B**) ssDNA assay and the (**C**) dsDNA assay. The amount of TREX1 protein used in the assays is indicated. The enzymatic activity of wild-type and mutated TREX1 proteins and the relative activity, which is shown as the ratio of the activity of the mutant to that of the wild type, are shown below each figure. Values are expressed as the mean (S.D.) of three independent experiments. The arrow in (C) indicates non-degraded, nicked dsDNA.

appeared on the fingers and toes in all seven cases; four of the seven also had lesions on the ears. In all cases the lesions were worse during the winter.

Recurrent fever was observed in seven patients (patients 1, 2, 4, 5, 8, 9 and 13). Regarding articular diseases, patient 4 suffered from scoliosis and a hip dislocation, and patient 10 had arthritis. Patients 7 and 9 suffered from hearing loss, and four patients (patients 2, 4, 8 and 14) had ophthalmological problems.

Patients 8 and 9, both harbouring *SAMHD1* mutations, fulfilled the ACR diagnostic criteria for SLE [29]. In addition, patient 10, who also harboured a *SAMHD1* mutation, was diagnosed with SS according to the Japanese criteria for SS [30].

TABLE 2 Clinical findings of Aicardi-Goutières syndrome patients

| Patient | Genotype | Age, years | Sex | GA, weeks | BW, g | Age at disease onset | Manifestations at disease onset | Developmental delay | Other neurological manifestations | Chilblain lesions | Extraneural manifestations |
|---|---|---|---|---|---|---|---|---|---|---|---|
| 1 | *TREX1* AD | 15 | F | 38 | 2840 | 23 d | Rash (extremities) | Moderate | Febrile convulsion | Yes | Recurrent fever, abdominal pain |
| 2 | *TREX1* AD | 15 | M | 39 | 2792 | 2 mo | Rash (extremities) | Severe | Hypotonia | Yes | Recurrent fever, conjunctivitis, posterior synechia |
| 3 | *TREX1* AD | 8 | M | 39 | 2828 | 4 mo | Delayed head control | Severe | None | Yes | None |
| 4 | *TREX1* AR | 19 | F | 38 | 2044 | 3 mo | Delayed head control | Severe | Microcephaly, spastic quadriplegia | Yes | Recurrent fever, oral ulcer, abdominal pain, visual impairment, scoliosis, hip dislocation, neurogenic bladder dysfunction |
| 5 | *TREX1* AR | 12 | M | 38 | 3000 | 18 d | Fever | Severe | Dystonia, hypotonia, microcephaly, febrile convulsion, mixed quadriplegia, startle reaction | Yes | Recurrent fever |
| 6 | *RNASEH2B* ? | 6 | F | Unknown | Unknown | 3 mo | Eye movement disorder | Severe | Dystonia, microcephaly | No | None |
| 7 | *RNASEH2A* AR | 2 | F | 36 | 1931 | 3 mo | Involuntary movement | Severe | Hypotonia (trunk), hypertonia (extremities), microcephaly, seizure | No | Hearing loss |
| 8 | *SAMHD1* AR | 14 | F | 40 | 2052 | 1 mo | Irritability | Severe | Dystonia, microcephaly, seizure | Yes | Recurrent fever, hepatosplenomegaly, glaucoma, corneal perforation |
| 9 | *SAMHD1* AR | 6 | F | 38 | 2534 | 5 d | Fever and feeding difficulties with thrombocytopenia | Severe | Dystonia, hypotonia, microcephaly | No | Recurrent fever, photosensitization, hearing loss |
| 10 | *SAMHD1* AR | 16 | M | 39 | 2330 | <4 mo | Irritability | Severe | Microcephaly | Yes | Arthritis |
| 11 | ND | 4 | M | 36 | 2780 | 4 d | Omphalitis with thrombocytopenia | Severe | Hypertonia, seizure, spastic quadriplegia | No | Idiopathic interstitial pneumonia |
| 12 | ND | 6 | M | 39 | 3290 | 6 mo | Developmental delay | Severe | Regression, dystonia, microcephaly | No | Atopic dermatitis |
| 13 | ND | 7 | F | 40 | 2144 | 0 d | Conjugate deviation | Severe | Dystonia, hypotonia, seizure, spastic paralysis | No | Recurrent fever |
| 14 | ND | 4 | F | 37 | 2056 | 0 d | Conjugate deviation | Severe | Regression, microcephaly, seizure, hemiplegia | No | Congenital cataract |

GA: gestational age; BW: birth weight; AR: autosomal recessive; AD: autosomal dominant; ND: not detected; M: male; F: female; d: day(s); mo: month(s). Patients 1–10 are the same as presented in Table 1. No significant mutations in six genes associated with AGS were detected in patients 11–14. Patients 13 and 14 are siblings.

FIG. 3 Clinical presentations of Aicardi-Goutières syndrome patients

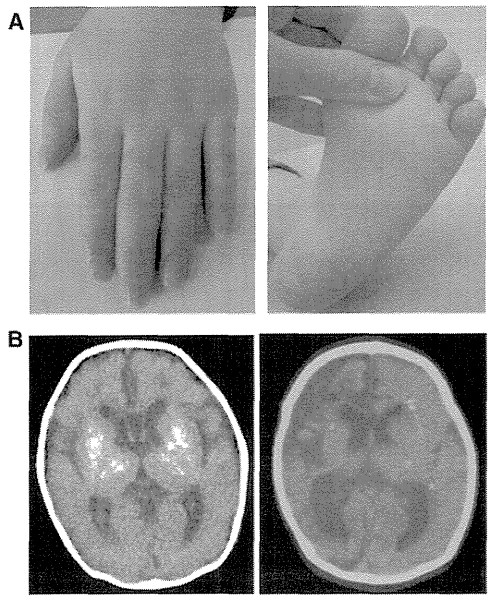


(**A**) Chilblain lesions observed in AGS patients. The left panel shows the hand of patient 1. The right panel shows the foot sole of patient 3. (**B**) Cranial calcifications on head CT scans. The left panel shows the head CT scan of patient 7 at the age of 4 months. The right panel shows head CT scan of patient 8 at the age of 3 months.

### Laboratory findings

All of the AGS patients examined showed at least one CSF abnormality, including lymphocytosis, elevated IFN-α levels or elevated neopterin levels (Table 3). All three patients harbouring dominant-type *TREX1* mutations (patients 1-3) showed elevated serum IFN-α levels at the age of ⩾7 years.

Seven patients showed elevated levels of serum autoantibodies: ANA in four cases (patients 8-10 and 12), anti-ssDNA antibodies in four cases (patients 5, 7, 9 and 10), anti-dsDNA antibodies in patients 5 and 9, anti-RNP antibodies in patients 8 and 10, anti-DNA antibody in patient 8, anti-SS-A antibody in patient 10 and anti-LKM1 antibody in patient 11. All three patients harbouring *SAMHD1* mutations showed increases in multiple autoantibody types. Other immunological findings included hypergammaglobulinaemia in patients 9-11 and hypocomplementaemia in patients 9 and 11.

Abnormal liver function was observed in nine cases (patients 4-6, 8-11, 13 and 14). Hematological abnormalities included thrombocytopenia in four cases (patients 8, 9, 11, and 13) and anaemia in patients 8 and 14. Regarding endocrine complications, we found moderate hypothyroidism in patients 1 and 9 and diabetes mellitus in patients 8 and 10.

### Imaging findings

CT scans revealed cranial calcifications in all 14 patients (Fig. 2B). Eleven patients (patients 1-7 and 9-12) had calcifications in the bilateral basal ganglia, and some had calcifications in the thalamus, periventricular lesions or cerebellar hemispheres. Eleven patients (patients 3-9 and 11-14) had white matter abnormalities. High-intensity signals were observed mainly in periventricular lesions, frontal lobes or temporal lobes on T2-weighted MRI scans. Brain atrophy was evident in all but patient 1; this patient showed only moderate developmental delay.

## Discussion

Here we present the results of the first nationwide survey of AGS patients conducted to examine the clinical manifestations and genotype-phenotype correlations of this disease. *RNASEH2B* is reported to be the most common gene associated with AGS (50 of 127 pedigrees) [3]; however, this mutation was identified at a significantly lower rate in the Japanese cohort ($P < 0.05$). The majority of the AGS patients in the present study harboured mutations in *TREX1* and *SAMHD1*. Although our cohort was small, the results suggest that the frequency of AGS gene mutations is variable in different ethnic populations.

AGS is usually inherited in an autosomal recessive manner, and previous studies have shown that consanguineous pedigrees are often involved [2, 3]. However, there was no consanguinity among our patients. Interestingly, we identified two patients harbouring *de novo* dominant-type *TREX1* mutations; this is a higher proportion than previously reported [3], since such patients are reported very rarely [2, 10-12]. AGS patients usually show severe neurological disabilities and rarely have children. Thus pedigrees are unhelpful when identifying *de novo* dominant-type AGS; however, the presence of parental consanguinity would facilitate the diagnosis of the more common recessive-type AGS. Since similar *de novo* mutations are expected to occur among different ethnic origins, we speculate that there might be more AGS patients harbouring *de novo* dominant-type mutations in other countries, regardless of the presence or absence of consanguinity.

The neurological symptoms shown by our AGS cohort were similar to those reported in previous studies, and included developmental delay, seizures, microcephaly, dystonia and hypotonia [2, 3]. The cohort also comprised a high percentage of patients with severe developmental delay, although AGS cases that are neurologically milder were recently described [2]. All of the patients in the present cohort presented with the first symptoms of the disease by the age of 6 months. This could be because the cohort harboured few *RNASEH2B* mutations, which are associated with less severe neurological findings and later-onset presentation [2, 3].

AGS is highly associated with type I IFN-related autoimmunity [2, 16]. SLE shows many similarities to AGS, and previous reports describe two patients with

TABLE 3 Laboratory findings of Aicardi-Goutières syndrome patients

| Patient | Genotype | CSF lymphocytosis | CSF elevated IFN-α | CSF elevated neopterin | Serum elevated IFN-α | Serum elevated autoantibody | Other clinical features |
|---|---|---|---|---|---|---|---|
| 1 | *TREX1* AD | n.d. | n.d. | n.d. | Yes (14 years) | None | Moderate hypothyroidism |
| 2 | *TREX1* AD | n.d. | n.d. | n.d. | Yes (13 years) | None | None |
| 3 | *TREX1* AD | Yes (1 years) | No (7 years) | No (7 years) | Yes (7 years) | None | None |
| 4 | *TREX1* AR | Yes (10 months) | Yes (2 years) | n.d. | n.d. | Unknown | Abnormal liver function |
| 5 | *TREX1* AR | Yes (23 days) | No (10 years) | n.d. | No (10 years) | Anti-ssDNA, anti-dsDNA | Abnormal liver function |
| 6 | *RNASEH2B* ? | Yes (8 months) | Yes (8 months) | n.d. | Yes (8 months) | None | Abnormal liver function |
| 7 | *RNASEH2A* AR | Yes (6 months) | Yes (6 months) | Yes (2 years) | No (6 months) | Anti-ssDNA | None |
| 8 | *SAMHD1* AR | Yes (2 months) | n.d. | n.d. | No (12 years) | ANA 1:20480, anti-DNA, anti-RNP | Thrombocytopenia, leucocytopenia, anaemia, abnormal liver function, diabetes mellitus |
| 9 | *SAMHD1* AR | Yes (9 months) | Yes (9 months) | n.d. | n.d. | ANA 1:640, anti-ssDNA, anti-dsDNA | Thrombocytopenia, abnormal liver function, hypocomplementaemia, hypergammaglobulinaemia, moderate hypothyroidism |
| 10 | *SAMHD1* AR | No (16 years) | n.d. | Yes (16 years) | n.d. | ANA 1:1280, anti-ssDNA, anti-RNP, anti-SS-A | Abnormal liver function, hypergammaglobulinaemia, diabetes mellitus |
| 11 | ND | No (11 months) | Yes (11 months) | n.d. | n.d. | Anti-LKM1 | Thrombocytopenia, abnormal liver function, hypocomplementaemia, hypergammaglobulinaemia |
| 12 | ND | No (3 years) | No (3 years) | Yes (3 years) | n.d. | ANA 1:320 | None |
| 13 | ND | n.d. | n.d. | n.d. | n.d. | Unknown | Thrombocytopenia, abnormal liver function |
| 14 | ND | Yes (4 days) | n.d. | n.d. | n.d. | None | Anaemia, abnormal liver function |

AR: autosomal recessive; AD: autosomal dominant; ND: not detected; n.d.: not done. Patients 1–14 are the same as those listed in Table 2. The age at which the data were collected is shown in parentheses.

TABLE 4 Summary of Aicardi-Goutières syndrome patients with dominant-type *TREX1* mutations

| Patient | Reference | Genotype | Mutation type | Ethnicity | Chilblain lesions | Developmental delay | Seizure | CSF elevated IFN-α | Serum elevated IFN-α |
|---|---|---|---|---|---|---|---|---|---|
| 1 | 19 | p.Asp18Asn | Het | Japanese | Yes | Moderate | FC only | n.d. | Yes (14 years) |
| 2 | — | p.His195Tyr | Het, *de novo* | Japanese | Yes | Severe | No | n.d. | Yes (13 years) |
| 3 | — | p.Asp200Asn | Mos, *de novo* | Japanese | Yes | Severe | No | No (7 years) | Yes (7 years) |
| — | 10 | p.Asp200Asn | Het, *de novo* | Scottish | Yes | Severe | No | Yes (3 years) | Undescribed |
| — | 2 | p.Asp200His | Het, *de novo* | German | Yes | Undescribed | Undescribed | Undescribed | Undescribed |
| — | 11 | p.Asp18Asn | Het, *de novo* | Undescribed | Yes | Relatively mild | No | Yes (14 years) | Yes (14 years) |
| — | 12 | p.Asp18His | Het, *de novo* | Undescribed | Yes | Severe | Undescribed | Yes (4 months) | Undescribed |

Het: heterozygous; Mos: mosaic; FC: febrile convulsion; n.d.: not done. The age at which the data were collected is shown in parentheses.

molecularly proven AGS that were also diagnosed with SLE, one harbouring a *SAMHD1* mutation and the other a *TREX1* mutation [2, 17]. In the present study, the first AGS patient complicated with SS, which is also known as a type I IFN-related disease [31], was identified, in addition to two AGS patients diagnosed with SLE. All three patients harboured *SAMHD1* mutations and tested positive for multiple autoantibodies. These findings suggest that, of all the genes associated with AGS, *SAMHD1* mutations may be most closely associated with autoimmunity. Further studies of this association might shed light on the pathophysiology of AGS and autoimmune diseases.

All five patients harbouring *TREX1* mutations had chilblain lesions, a frequency significantly greater than that observed for the rest of the cohort (2/9 patients; $P < 0.05$). However, no previous studies have reported that chilblain lesions are more common in AGS patients harbouring *TREX1* mutations than in those harbouring other gene mutations. Thus we paid attention to the three patients harbouring dominant-type *TREX1* mutations. The clinical features of seven AGS patients with dominant-type *TREX1* mutations, who consist of the three reported herein and four additional cases reported in the literature, are presented in Table 4 [2, 10–12]. Notably, all seven cases had chilblain lesions, which is a significantly higher proportion than that observed in AGS patients as a whole (43% of 123 patients; $P < 0.01$) [3]. Besides AGS, heterozygous *TREX1* mutations are also associated with FCL, which presents with skin symptoms alone [10, 18, 19, 32]. Since dominant-type *TREX1* mutations are more likely to cause chilblains, it would be interesting to examine the differences in the underlying molecular mechanisms.

Although IFN-α levels in the CSF of AGS patients usually normalize during the first few years [3], serum IFN-α levels have not been studied extensively. We found that AGS patients harbouring dominant-type *TREX1* mutations tended to show persistent increases in serum IFN-α levels, even after they became older (Table 4). Previous reports have shown that patients receiving type I IFN present with vasculitic lesions that are similar to the chilblain lesions seen in AGS patients [33, 34]. Therefore we speculate that the chilblain lesions observed in AGS patients harbouring dominant-type *TREX1* mutations are related to persistently high serum IFN-α levels. Since the data on serum IFN-α levels of AGS patients are limited, further studies of more AGS cases from different ethnic backgrounds are needed to confirm the relationship between chilblains and IFN-α levels.

The dimeric protein, TREX1, is a major component of the 3′–5′ exonucleases in mammalian cells and functions to eliminate ssDNA and degrade nicked genomic DNA [6, 35, 36]. A previous study showed that *TREX1* mutations causing dominant-type AGS are localized to Asp18 and Asp200, which are highly conserved $Mg^{2+}$-coordinating aspartate residues required for catalytic function (Table 4) [37]. The heterozygous mutations p.Asp18Asn, p.Asp200Asn and p.Asp200His cause loss of function and exert dominant negative effects on the wild type [38, 39]. We identified a novel heterozygous *TREX1* mutation, p.His195Tyr, in our cohort. The exonuclease assays revealed that $TREX1^{p.His195Tyr}$ showed defective enzymatic activity, similar to $TREX1^{p.Asp18Asn}$ and $TREX1^{p.Asp200Asn}$. Although we did not generate heterodimers to prove the dominant negative effect, we identified a third TREX1 residue, His195, which causes AGS in a dominant-type manner when mutated.

We also identified the first AGS patient harbouring a somatic mosaicism for a *TREX1* mutation, suggesting that mutated cells could cause AGS, even when co-existing with normal cells. This mosaicism is consistent with the hypothesis that IFN-α released from non-hematopoietic cells acts in a paracrine fashion and plays a vital role in the pathogenesis of AGS [40]. The finding that the

frequency of the mosaicism was similar in every cell lineage or tissue tested suggests that neural cells would also show a similar frequency. From a diagnostic point of view, clinical AGS patients showing an even lower rate of mosaicism in *de novo* dominant-type *TREX1* mutations might be missed by conventional direct sequencing, like some reported cases of cryopyrin-associated periodic syndrome [22, 23, 41, 42].

In conclusion, the present nationwide survey identified more sporadic AGS cases harbouring *de novo* dominant-type *TREX1* mutations than expected. By exploring the genotype–phenotype correlations, we also observed a strong association between dominant-type *TREX1* mutations and chilblain lesions, as well as between *SAMHD1* mutations and autoimmunity. These findings need to be confirmed in AGS patients from different ethnic backgrounds. Nonetheless, these findings emphasize that rheumatologists need to pay attention to possible sporadic AGS cases that present with neurological disorders and autoimmune manifestations, even from non-consanguineous families.

**Rheumatology key messages**

- A strong association between dominant-type *TREX1* mutations and chilblain lesions was observed in Aicardi-Goutières syndrome patients.
- Special attention should be paid to Aicardi-Goutières syndrome patients with *de novo* dominant-type *TREX1* mutations.

## Acknowledgements

We are grateful to Y. Takaoka (Kyoto University, Kyoto, Japan) for technical assistance and to F. Perrino and C. Orebaugh (Wake Forest School of Medicine, Winston-Salem, NC, USA) for helpful suggestions regarding the ssDNA assay.

*Funding*: This work was supported by grants from the Health Labour Sciences Research Grant for Research on Intractable Diseases from the Ministry of Health, Labour and Welfare of Japan (H22-nanchi-ippan-123, H23-nanchi-ippan-096) and the Ministry of Education, Culture, Sports, Science and Technology of Japan (24390263).

*Disclosure statement*: The authors have declared no conflicts of interest.

## References

1 Chahwan C, Chahwan R. Aicardi-Goutieres syndrome: from patients to genes and beyond. Clin Genet 2012;81:413–20.

2 Ramantani G, Kohlhase J, Hertzberg C *et al.* Expanding the phenotypic spectrum of lupus erythematosus in Aicardi-Goutières syndrome. Arthritis Rheum 2010;62:1469–77.

3 Rice G, Patrick T, Parmar R *et al.* Clinical and molecular phenotype of Aicardi-Goutieres syndrome. Am J Hum Genet 2007;81:713–25.

4 Orcesi S, La Piana R, Fazzi E. Aicardi-Goutieres syndrome. Br Med Bull 2009;89:183–201.

5 Blau N, Bonafé L, Krägeloh-Mann I *et al.* Cerebrospinal fluid pterins and folates in Aicardi-Goutières syndrome: a new phenotype. Neurology 2003;61:642–7.

6 Crow YJ, Hayward BE, Parmar R *et al.* Mutations in the gene encoding the 3′-5′ DNA exonuclease TREX1 cause Aicardi-Goutières syndrome at the AGS1 locus. Nat Genet 2006;38:917–20.

7 Crow YJ, Leitch A, Hayward BE *et al.* Mutations in genes encoding ribonuclease H2 subunits cause Aicardi-Goutières syndrome and mimic congenital viral brain infection. Nat Genet 2006;38:910–6.

8 Rice GI, Bond J, Asipu A *et al.* Mutations involved in Aicardi-Goutières syndrome implicate SAMHD1 as regulator of the innate immune response. Nat Genet 2009;41:829–32.

9 Rice GI, Kasher PR, Forte GM *et al.* Mutations in ADAR1 cause Aicardi-Goutières syndrome associated with a type I interferon signature. Nat Genet 2012;44:1243–8.

10 Rice G, Newman WG, Dean J *et al.* Heterozygous mutations in TREX1 cause familial chilblain lupus and dominant Aicardi-Goutieres syndrome. Am J Hum Genet 2007;80:811–5.

11 Haaxma CA, Crow YJ, van Steensel MA *et al.* A de novo p.Asp18Asn mutation in TREX1 in a patient with Aicardi-Goutières syndrome. Am J Med Genet A 2010;152A:2612–7.

12 Tüngler V, Silver RM, Walkenhorst H *et al.* Inherited or de novo mutation affecting aspartate 18 of TREX1 results in either familial chilblain lupus or Aicardi-Goutières syndrome. Br J Dermatol 2012;167:212–4.

13 Crow YJ. Type I interferonopathies: a novel set of inborn errors of immunity. Ann N Y Acad Sci 2011;1238:91–8.

14 Obermoser G, Pascual V. The interferon-alpha signature of systemic lupus erythematosus. Lupus 2010;19:1012–9.

15 Lee-Kirsch MA, Gong M, Chowdhury D *et al.* Mutations in the gene encoding the 3′-5′ DNA exonuclease TREX1 are associated with systemic lupus erythematosus. Nat Genet 2007;39:1065–7.

16 Cheng MH, Anderson MS. Monogenic autoimmunity. Annu Rev Immunol 2012;30:393–427.

17 Ramantani G, Häusler M, Niggemann P *et al.* Aicardi-Goutières syndrome and systemic lupus erythematosus (SLE) in a 12-year-old boy with SAMHD1 mutations. J Child Neurol 2011;26:1425–8.

18 Lee-Kirsch MA, Gong M, Schulz H *et al.* Familial chilblain lupus, a monogenic form of cutaneous lupus erythematosus, maps to chromosome 3p. Am J Hum Genet 2006;79:731–7.

19 Abe J, Izawa K, Nishikomori R *et al.* Heterozygous TREX1 p.Asp18Asn mutation can cause variable neurological symptoms in a family with Aicardi-Goutieres syndrome/familial chilblain lupus. Rheumatology 2013;52:406–8.

20 Shintaku H, Asada M, Sawada Y. Diagnosis and treatment of 6-pyruvoyl-tetrahydropterin synthase deficiency. Brain Dev 2000;22(Suppl 1):S118–21.

21 Nishikomori R, Akutagawa H, Maruyama K *et al*. X-linked ectodermal dysplasia and immunodeficiency caused by reversion mosaicism of NEMO reveals a critical role for NEMO in human T-cell development and/or survival. Blood 2004;103:4565–72.

22 Izawa K, Hijikata A, Tanaka N *et al*. Detection of base substitution-type somatic mosaicism of the NLRP3 gene with >99.9% statistical confidence by massively parallel sequencing. DNA Res 2012;19:143–52.

23 Tanaka N, Izawa K, Saito MK *et al*. High incidence of NLRP3 somatic mosaicism in patients with chronic infantile neurologic, cutaneous, articular syndrome: results of an international multicenter collaborative study. Arthritis Rheum 2011;63:3625–32.

24 Orebaugh CD, Fye JM, Harvey S *et al*. The TREX1 exonuclease R114H mutation in Aicardi-Goutières syndrome and lupus reveals dimeric structure requirements for DNA degradation activity. J Biol Chem 2011;286:40246–54.

25 Brucet M, Querol-Audí J, Serra M *et al*. Structure of the dimeric exonuclease TREX1 in complex with DNA displays a proline-rich binding site for WW Domains. J Biol Chem 2007;282:14547–57.

26 Brucet M, Querol-Audí J, Bertlik K *et al*. Structural and biochemical studies of TREX1 inhibition by metals. Identification of a new active histidine conserved in DEDDh exonucleases. Protein Sci 2008;17:2059–69.

27 Bailey SL, Harvey S, Perrino FW *et al*. Defects in DNA degradation revealed in crystal structures of TREX1 exonuclease mutations linked to autoimmune disease. DNA Repair (Amst) 2012;11:65–73.

28 Kavanagh D, Spitzer D, Kothari PH *et al*. New roles for the major human 3′-5′ exonuclease TREX1 in human disease. Cell Cycle 2008;7:1718–25.

29 Tan EM, Cohen AS, Fries JF *et al*. The 1982 revised criteria for the classification of systemic lupus erythematosus. Arthritis Rheum 1982;25:1271–7.

30 Miyawaki S. Revised Japan criteria for Sjögren syndrome. Ryumachi 2000;40:48–53.

31 Yao Y, Liu Z, Jallal B *et al*. Type I interferons in Sjögren's syndrome. Autoimmun Rev 2013;12:558–66.

32 Lee-Kirsch MA, Chowdhury D, Harvey S *et al*. A mutation in TREX1 that impairs susceptibility to granzyme A-mediated cell death underlies familial chilblain lupus. J Mol Med (Berl) 2007;85:531–7.

33 Bachmeyer C, Farge D, Gluckman E *et al*. Raynaud's phenomenon and digital necrosis induced by interferon-alpha. Br J Dermatol 1996;135:481–3.

34 Campo-Voegeli A, Estrach T, Marti RM *et al*. Acrocyanosis induced by interferon alpha(2a). Dermatology 1998;196:361–3.

35 Stetson DB, Ko JS, Heidmann T *et al*. Trex1 prevents cell-intrinsic initiation of autoimmunity. Cell 2008;134:587–98.

36 Chowdhury D, Beresford PJ, Zhu P *et al*. The exonuclease TREX1 is in the SET complex and acts in concert with NM23-H1 to degrade DNA during granzyme A-mediated cell death. Mol Cell 2006;23:133–42.

37 de Silva U, Choudhury S, Bailey SL *et al*. The crystal structure of TREX1 explains the 3′ nucleotide specificity and reveals a polyproline II helix for protein partnering. J Biol Chem 2007;282:10537–43.

38 Lehtinen DA, Harvey S, Mulcahy MJ *et al*. The TREX1 double-stranded DNA degradation activity is defective in dominant mutations associated with autoimmune disease. J Biol Chem 2008;283:31649–56.

39 Fye JM, Orebaugh CD, Coffin SR *et al*. Dominant mutations of the TREX1 exonuclease gene in lupus and Aicardi-Goutieres syndrome. J Biol Chem 2011;286:32373–82.

40 Gall A, Treuting P, Elkon KB *et al*. Autoimmunity initiates in nonhematopoietic cells and progresses via lymphocytes in an interferon-dependent autoimmune disease. Immunity 2012;36:120–31.

41 Saito M, Fujisawa A, Nishikomori R *et al*. Somatic mosaicism of CIAS1 in a patient with chronic infantile neurologic, cutaneous, articular syndrome. Arthritis Rheum 2005;52:3579–85.

42 Saito M, Nishikomori R, Kambe N *et al*. Disease-associated CIAS1 mutations induce monocyte death, revealing low-level mosaicism in mutation-negative cryopyrin-associated periodic syndrome patients. Blood 2008;111:2132–41.

OPEN ACCESS Freely available online

PLOS | ONE

# Robust and Highly-Efficient Differentiation of Functional Monocytic Cells from Human Pluripotent Stem Cells under Serum- and Feeder Cell-Free Conditions

**Masakatsu D. Yanagimachi[1,4], Akira Niwa[1], Takayuki Tanaka[1], Fumiko Honda-Ozaki[1], Seiko Nishimoto[1], Yuuki Murata[3], Takahiro Yasumi[3], Jun Ito[1], Shota Tomida[1], Koichi Oshima[1], Isao Asaka[2], Hiroaki Goto[4], Toshio Heike[3], Tatsutoshi Nakahata[1], Megumu K. Saito[1]***

**1** Department of Clinilcal Application, Center for iPS Cell Research and Application, Kyoto University, Kyoto, Japan, **2** Department of Fundamental Cell Technology, Center for iPS Cell Research and Application, Kyoto University, Kyoto, Japan, **3** Department of Pediatrics, Kyoto University Graduate School of Medicine, Kyoto, Japan, **4** Department of Pediatrics, Yokohama City University Graduate School of Medicine, Yokohama, Japan

## Abstract

Monocytic lineage cells (monocytes, macrophages and dendritic cells) play important roles in immune responses and are involved in various pathological conditions. The development of monocytic cells from human embryonic stem cells (ESCs) and induced pluripotent stem cells (iPSCs) is of particular interest because it provides an unlimited cell source for clinical application and basic research on disease pathology. Although the methods for monocytic cell differentiation from ESCs/iPSCs using embryonic body or feeder co-culture systems have already been established, these methods depend on the use of xenogeneic materials and, therefore, have a relatively poor-reproducibility. Here, we established a robust and highly-efficient method to differentiate functional monocytic cells from ESCs/iPSCs under serum- and feeder cell-free conditions. This method produced $1.3\times10^6\pm0.3\times10^6$ floating monocytes from approximately 30 clusters of ESCs/iPSCs 5–6 times per course of differentiation. Such monocytes could be differentiated into functional macrophages and dendritic cells. This method should be useful for regenerative medicine, disease-specific iPSC studies and drug discovery.

**Citation:** Yanagimachi MD, Niwa A, Tanaka T, Honda-Ozaki F, Nishimoto S, et al. (2013) Robust and Highly-Efficient Differentiation of Functional Monocytic Cells from Human Pluripotent Stem Cells under Serum- and Feeder Cell-Free Conditions. PLoS ONE 8(4): e59243. doi:10.1371/journal.pone.0059243

**Editor:** Katriina Aalto-Setala, University of Tampere, Finland

**Received** August 14, 2012; **Accepted** February 13, 2013; **Published** April 3, 2013



**Funding:** Funding was provided by grants from the Ministry of Health, Labour and Welfare to TN, a grant from the Ministry of Education, Culture, Sports, Science and Technology (MEXT) to TN, grants from the Leading Project of MEXT to TN, a grant from Funding Program for World-Leading Innovative Research and Development on Science and Technology (FIRST Program) of Japan Society for the Promotion of Science (JSPS) to TN, grants from JSPS to TN and MKS, grants from the Takeda foundation, Mitsubishi Pharma Research Foundation and Suzuken memorial foundation to MKS and grants from Grants-in-Aid for Scientific Research from Japan Society for the Promotion of Science from the Ministry of Education, Culture, Sports, Science, and Technology of Japan to MDY. The funders had no role in study design, data collection and analysis, decision to publish, or preparation of the manuscript.

**Competing Interests:** The authors have declared that no competing interests exist.

* E-mail: msaito@cira.kyoto-u.ac.jp

## Introduction

Monocytic lineage cells, such as monocytes, macrophages and dendritic cells (DCs), are central to immune responses and play key roles in various pathological conditions. [1–2] Monocytes are the myeloid progeny of hematopoietic stem/progenitor cells [3]; they are a type of mononuclear cell circulating in the bloodstream and act as gatekeepers in innate immunity. While they replenish macrophages and DCs, monocytes themselves respond to various inflammatory stimuli by migrating into inflamed tissues, phagocytosing pathological small particles and producing proinflammatory cytokines and chemokines. Therefore, monocytes not only contribute to host defense against pathogenic microorganisms, but are closely associated with the pathogenesis of chronic sterile inflammation. [4] Macrophages reside in tissues and robustly phagocytose microorganisms and cellular debris. One of the important hallmarks of monocytic lineage cells is their functional plasticity. In response to cytokines and microbial products, macrophages polarize into functionally distinct M1 and M2 cells. [5] Classically activated M1 macrophages are induced by interferon-γ (IFNγ), while alternatively activated M2 macrophages can be induced by IL-4 and IL-13. [2,5] M1 macrophages are generally characterized by high production of proinflammatory cytokines, while M2 are characterized by high production of anti-inflammatory cytokines. DCs are the most powerful antigen-presenting cells and have an indispensable role for the activation of T lymphocytes. Because of their ability to mediate communication between innate and acquired immunity, ex vivo expansion of DCs is expected to be a useful source of material for cancer immunotherapies, such as DC-based vaccines. [6–7] Moreover, recent reports of monocyte and/or DC deficiencies highlight the importance of understanding their development in humans. [8] However, there have been technical limitations for tracing the development of human monocytic cells, or for propagating them ex vivo.

Human embryonic stem cells (ESCs) and induced pluripotent stem cells (iPSCs) are undifferentiated pluripotent cells that can be propagated indefinitely. [9–11] The development of monocytic cells from these pluripotent cells is of particular interest because it would provide an unlimited source of these cells for clinical applications and the examination of disease pathologies. Although the methods for hematopoietic differentiation from ESCs/iPSCs

using embryonic body or feeder co-culture systems have already been established, [12] these methods usually depend on xenogeneic feeder cells and/or animal- or human-derived serum, and therefore have a relatively poor-reproducibility. For instance, batch-to-batch variability of serum or feeder cells can influence the characteristics of *in vitro* differentiated DCs. [13] Here, we describe a novel serum- and feeder cell-free method that robustly and repetitively produces monocytic lineage cells from human ESCs/iPSCs.

## Materials and Methods

### Cell Culture

This study used human ESCs (cell line: KhES1) and iPSCs (cell lines: 201B7, 253G4, CIRA188Ai-W2, and CB-A11). [10,14–15] 201B7, 253G4 [10] and CIRA188Ai-W2 [15] were previously described. A human ES cell line KhES1 was kindly provided by Dr. Norio Nakatsuji. Human iPS cell lines 201B7 and 253G4 were kindly provided by Dr. Shinya Yamanaka. CB-A11 was established from cord-blood mononuclear cells by using episomal vectors. [16] These ESCs/iPSCs were maintained on tissue culture dishes coated with growth factor-reduced Matrigel (Becton-Dickinson) in mTeSR1 serum-free medium (STEMCELL Technologies).

### Monocytic Lineage Cell Differentiation Method

The monocytic lineage differentiation protocol was modified from a previously established hematopoietic differentiation protocol (Figure 1). [17] The protocol consists of 5 sequential steps by which mature MPs and DCs are differentiated from human pluripotent cells in a stepwise manner. In the first step, primitive streak cells were induced from undifferentiated ESCs/iPSCs, which were then differentiated into hemangioblast-like hematopoietic progenitors in the second step. In step 3, expanded hematopoietic progenitors were committed towards initial myeloid differentiation, and then differentiated into the monocytic lineage in step 4. Finally, $CD14^+$ monocytes were differentiated into either MPs or DCs in step 5. The cytokines used in this study were purchased from R&D systems.

**Step 1: induction of primitive streak-like cells from undifferentiated human ES/iPS cells with BMP4.** BMP4 is an important molecule for the initial stage of mesodermal commitment of pluripotent stem cells in vitro. [17] Undifferentiated ESCs/iPSCs colonies were disseminated onto a 100 mm culture dish coated with growth factor-reduced Matrigel in mTeSR1 medium at a density of about 30 colonies per dish. Individual colonies were grown to a diameter of approximately 1 mm (Day 0), and BMP4 (80 ng/mL) was added to the mTeSR1 medium.

**Step 2: generation of $KDR^+CD34^+$ hemangioblast-like cells with VEGF, basic FGF and SCF.** VEGF and SCF have been reported to be important cytokines for development of hemoangiogenic progenitors. [18–19] In this step, we also added basic FGF which enhances the development of mesodermal hematopoietic progenitors. [18,20] The mTeSR1 medium was replaced by StemPro-34 serum-free medium (Gibco) containing 2 mM glutamax (Invitrogen) on day 4, and then was supplemented with the step-2 cytokine cocktail composed of VEGF (80 ng/mL), basic FGF (25 ng/ml), and SCF (100 ng/mL).

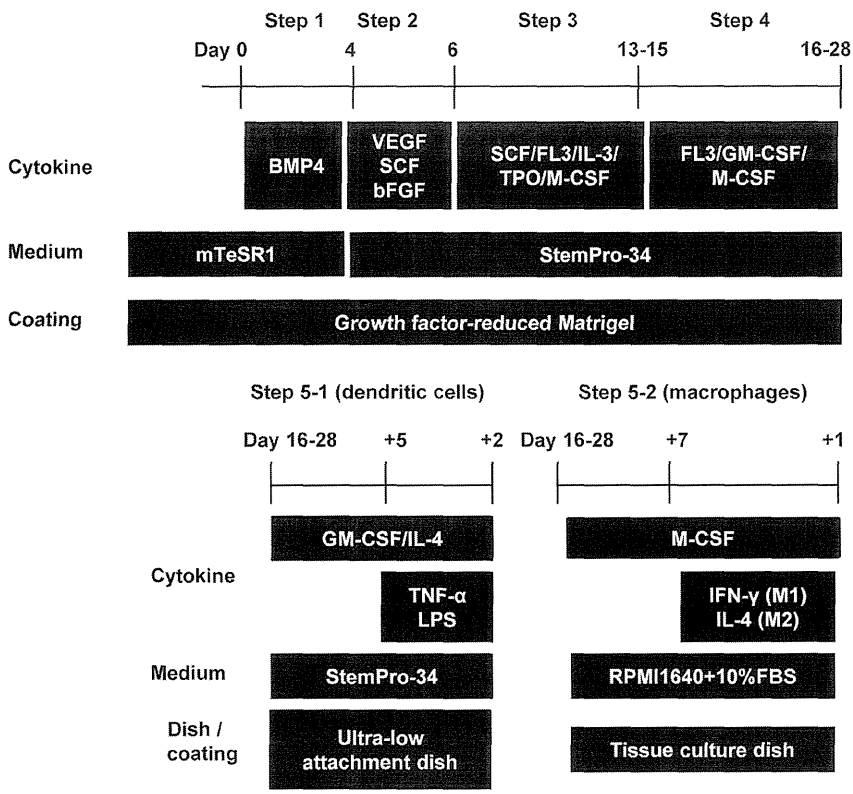


**Figure 1. Protocol for monocytic lineage cell differentiation from human pluripotent stem cells.** The protocol is composed of 5 steps. CD14-positive cells that are sorted between step-4 are differentiated into dendritic cells by step 5-1 or into macrophages by step 5-2. FL-3: Flt-3 ligand, TPO: Thrombopoietin.
doi:10.1371/journal.pone.0059243.g001

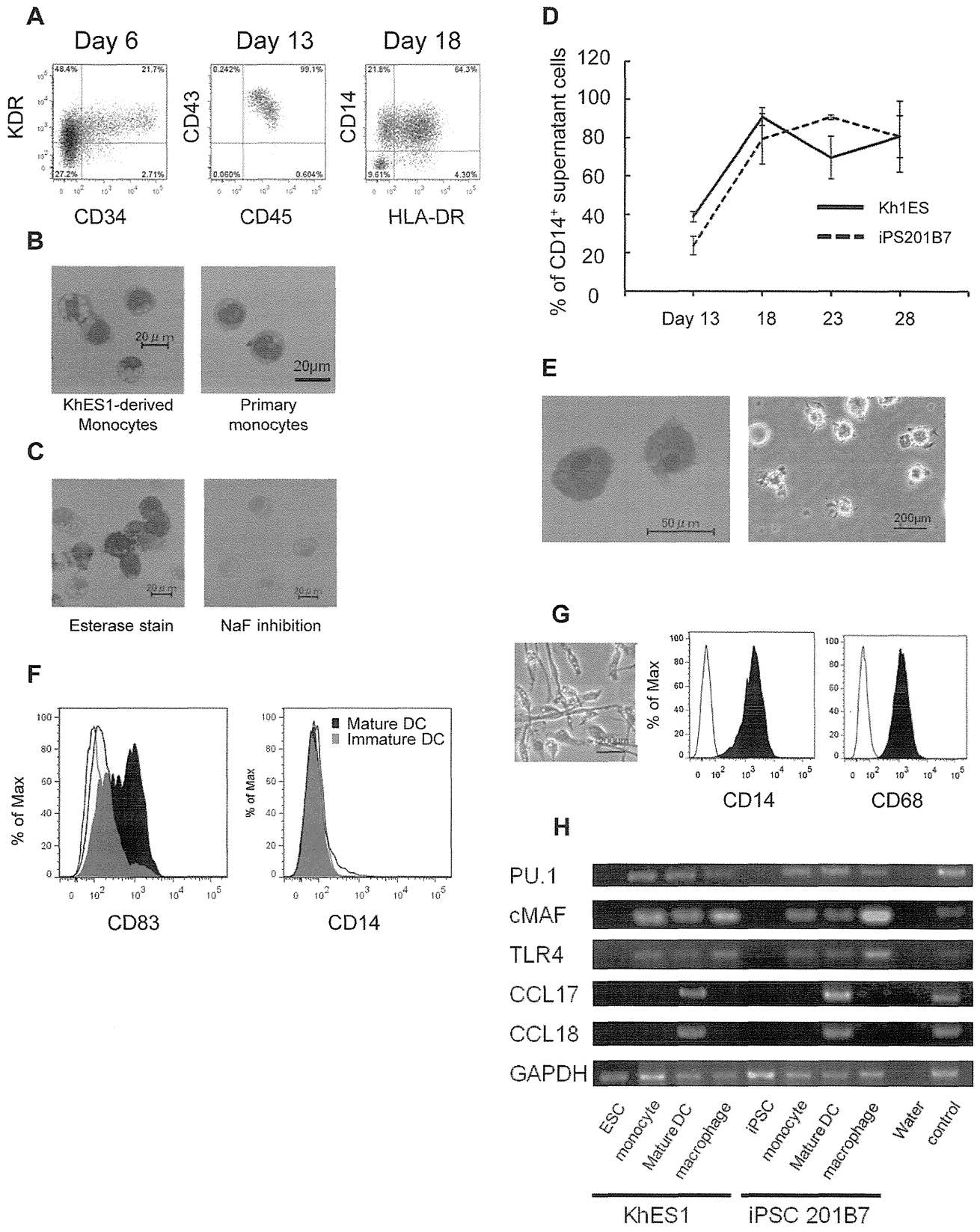


**Figure 2. Phenotype analysis and gene expression pattern of monocytic lineage cells derived from pluripotent stem cells.** (A) Flow cytometric analysis of monocytic lineage cells derived sequentially from pluripotent stem cells. An analysis of adherent cells on day 6 and supernatant cells on day 13 and 18 is shown. (B) May-Giemsa staining of $CD14^+$ monocyte-like cells derived from KhES1 on day 16 (left) and primary human monocytes (right). (C) Esterase staining for $CD14^+$ monocyte-like cells derived from KhES1 on day 16. (D) The percentage of $CD14^+$ cells within the total floating cells derived from KhES1/iPS-201B7 was evaluated from day 13 to day 28. (E) May-Giemsa staining (left) and phase contrast image (right)

of mature DCs derived from pluripotent stem cells. (F) Flow cytometric analysis of immature/mature DCs derived from pluripotent stem cells. (G) Phase contrast image and flow cytometric analysis of macrophages derived from pluripotent stem cells.(H) RT-PCR analysis of monocytic lineage cells derived from KhES1/iPS-201B7 clones for expression of monocytic lineage marker genes (*PU.1, c-MAF, TLR4, CCL17* and *CCL18*). Peripheral blood monocytes and peripheral blood monocyte-derived mature DCs were used as positive controls.(A–C, E–G) The data from KhES1-derived cells are shown as representative.
doi:10.1371/journal.pone.0059243.g002

**Step 3: generation of hematopoietic cells with hematopoietic cytokines.** The cytokines in StemPro-34 medium were switched to the step-3 cytokine cocktail composed of SCF (50 ng/mL), IL-3 (50 ng/mL), TPO (Thrombopoietin) (5 ng/mL), M-CSF (50 ng/mL), and Flt-3 ligand (50 ng/mL), on day 6. Thereafter, the medium was changed on day 10.

**Step 4: monocytic lineage-directed differentiation with Flt-3 ligand, GM-CSF and M-CSF.** The cytokines in StemPro-34 medium were switched to the step-4 cytokine cocktail composed of Flt-3 ligand (50 ng/mL), GM-CSF (25 ng/mL), and M-CSF (50 ng/mL) on day 13–15. The medium was changed every 3–4 days. The $CD14^+$ monocytic lineage-directed cell fraction in supernatant was positively sorted by autoMACS pro (Miltenyi Biotec) with CD14 MicroBeads (Miltenyi Biotec) on days 15–28.

**Step 5: differentiation into DCs (step 5-1) and MPs (step 5-2) from $CD14^+$ monocytic lineage-cells.** $CD14^+$ cells sorted by autoMACS pro ($1.5\times10^6$ cells per well in a 6-well plate with Ultra-Low Attachment Surface (CORNING)) were cultured in StemPro-34 medium supplemented with GM-CSF (25 ng/mL) and IL-4 (40 ng/mL), with a medium change 4 days later, for differentiation into DCs (step 5-1). LPS (100 ng/mL, InvivoGen) and TNFα (0.2 ng/mL) were added for the last 2 days of the 7 day DC differentiation culture to promote maturation of DCs. $CD14^+$ cells ($1.5\times10^6$ cells per well in a 6-well tissue culture plate) were cultured in RPMI-1640 medium (Sigma) supplemented with 10%

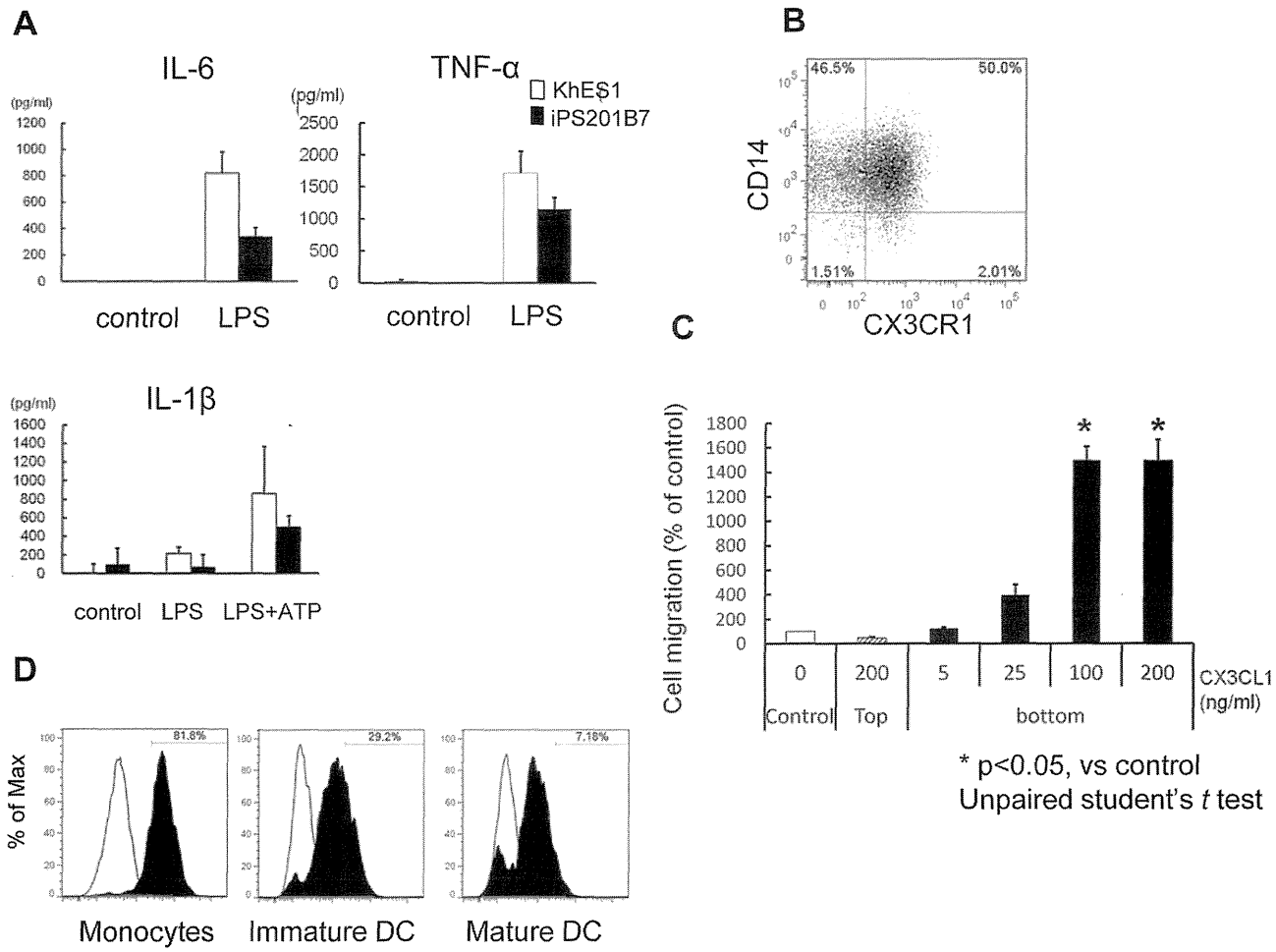


**Figure 3. Functional assays for monocytes derived from pluripotent stem cells.** (A) The levels of IL-6 and TNFα in supernatants of PS-Mo culture medium 4 hours after LPS stimulation. The levels of IL-1β were measured 4 hours after LPS stimulation with/without an additional 30-minute ATP stimulation. (B) Flow cytometric analysis of CX3CR1 on PS-Mo. (C) Chemotaxis assay of PS-Mo for CX3CL1 (fractalkine) using a trans-well migration assay. After the addition of CX3CL1 into either the bottom or top of the trans-well chamber, PS-Mo were applied and incubated for 5 hours at 37°C. (D) Antigen uptake was evaluated in monocytes, immature DCs and mature DCs derived from pluripotent stem cells by examining the fluorescence intensity of Alexa fluor 488-conjugated ovalbumin 45 minute after incubation at 37°C (black). Control samples (white) were kept on ice. (B–D) The data of KhES1-derived cells are shown as representative. PS-Mo: monocyte derived from pluripotent stem cells.
doi:10.1371/journal.pone.0059243.g003

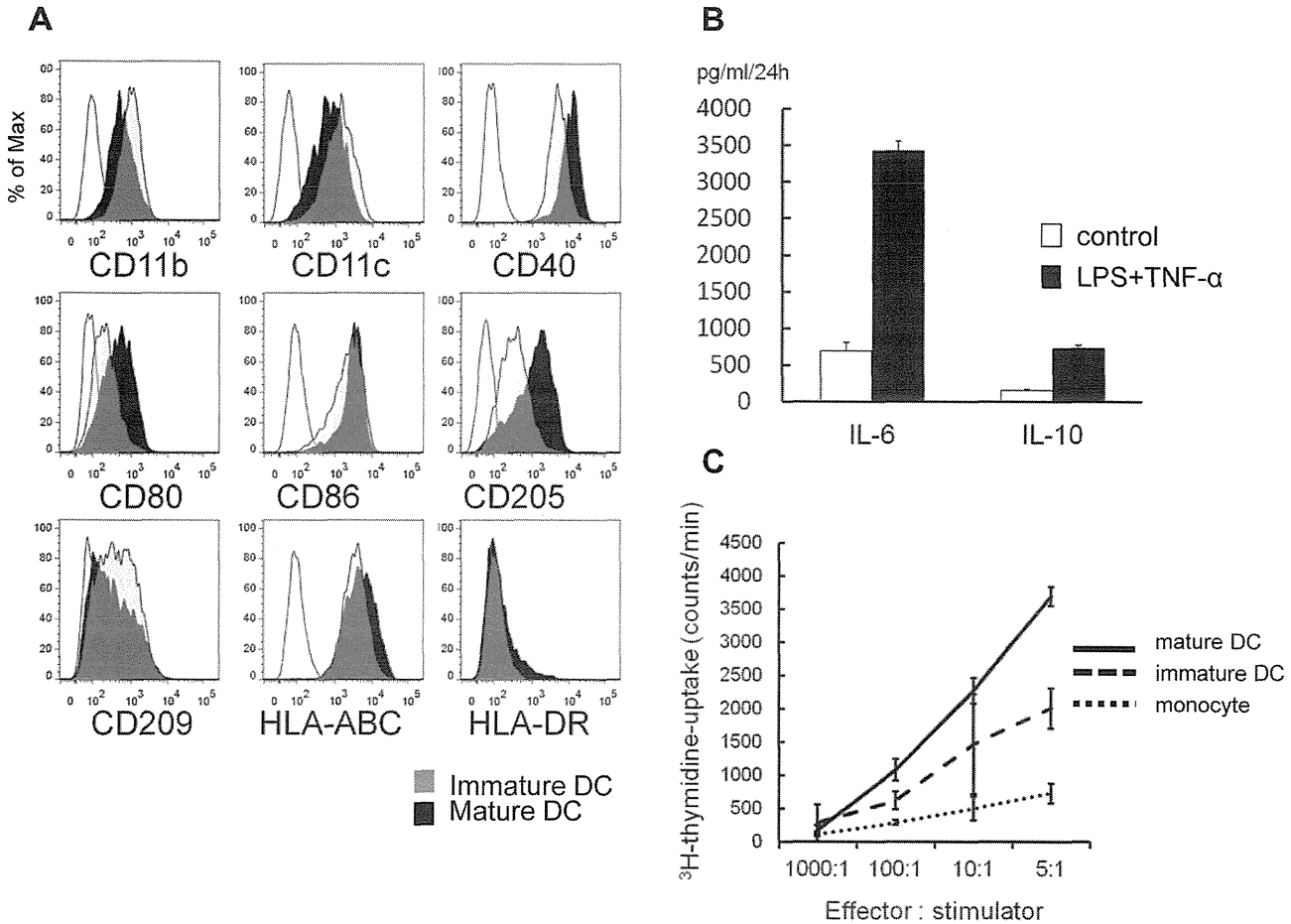


**Figure 4. Functional assays for dendritic cells derived from pluripotent stem cells.** (A) Flow cytometric analysis of immature/mature DCs derived from pluripotent stem cells. (B) The levels of IL-10 and TNFα in supernatants of culture medium with PS-DCs 24 hours after LPS stimulation. (C) The proliferation of allogeneic naïve T cells ($1\times10^5$ cells per well) co-cultured with 40 Gy-irradiated stimulator cells for 3 days was evaluated. The proliferation of naïve T cells in the last 16 hours was measured by $^3$H-thymidine uptake. (A–C) The data of KhES1-derived cells are shown as representative.

doi:10.1371/journal.pone.0059243.g004

fetal bovine serum (FBS) and M-CSF (100 ng/mL) for 7 days with a medium change at day 4, for differentiation into macrophages (step 5-2). IFNγ (20 ng/ml) or IL-4 (20 ng/ml) was added for another day to promote differentiation into M1 or M2 macrophages, respectively.

## Flow Cytometric Analysis

Flow cytometric analysis data were collected using the MACS Quant™ Analyzer (Miltenyi Biotec) and then analyzed utilizing the FlowJo software package (Treestar). The following antibodies were purchased from BD Biosciences: CD11b-FITC, CD11c-APC, CD34-PE, CD40-PE, CD43-FITC, CD80-PE, CD83-PE, CD86-FITC, CD205-Alexa fluor 647, CD206-FITC, CD209-PE, HLA-ABC-FITC and HLA-DR-FITC. CD14-APC and CD45-APC antibodies were purchased from Beckman Coulter. CD163-APC antibody was purchased from R&D systems. KDR (CD309)-Alexa fluor 647 and CX3CR1-PE antibodies were purchased from Biolegend.

## May-Giemsa Staining and Esterase Staining

Cells were seeded onto glass slides by CYTOSPIN 4 (Thermo Scientific) and stained with May-Grunwald and Giemsa staining solution (MERCK) and Esterase staining solution (Muto pure chemicals) following the manufacturer's instructions.

## RNA Extraction and RT-PCR Analysis

RNA samples were prepared using the RNeasy mini kit (Qiagen) following the manufacturer's instructions. Typically, 500 ng of total RNA were subjected to reverse transcription (RT) with a Sensiscript-RT kit (Qiagen). RT-PCR was performed for the evaluation of the expression of monocytic lineage marker genes such as *PU.1*, *MAF*, *TLR4*, *CCL17* and *CCL18* using the primers in **Table S1**. [21–22] Peripheral blood monocyte-derived mature DCs/macrophages were generated from peripheral $CD14^+$ monocytes using the step 5-1/5-2 cytokine cocktails in 10% FBS-supplemented RPMI-1640 for use as positive controls.

## Cytokine Assay

Concentrations of cytokines (IL-1β, IL-6, IL-10, IL-12p70 and TNFα) in supernatants were analyzed with FlowCytomix kits (Bender MedSystems) following the manufacturer's instructions. The IL-1β, IL-6 and TNFα levels in the culture supernatants of pluripotent cell-derived monocytes (PS-Mo) were analyzed in three settings, (1) culture in RPMI-1640 medium supplemented with 10% FBS and LPS (100 ng/ml) for 4.5 hours, (2) as in (1) but with

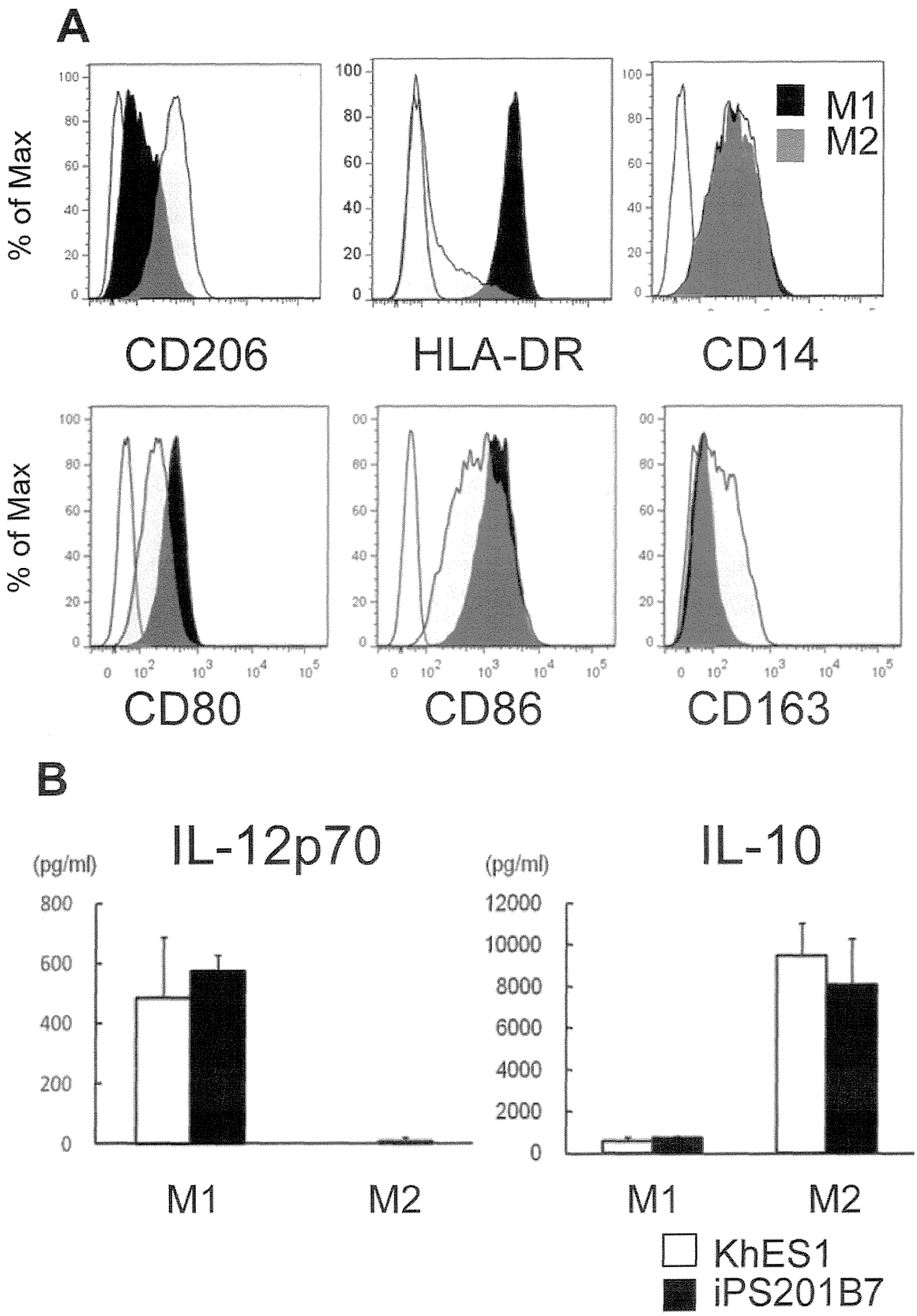


**Figure 5. Functional assays for M1/M2 macrophages derived from pluripotent stem cells.** (A) Flow cytometric analysis of M1/M2 macrophages derived from pluripotent stem cells. (B) The levels of IL-12p70 and IL-10 in supernatants of culture medium with M1/M2 macrophages derived from pluripotent stem cells 24 hours after LPS stimulation. The data of KhES1-derived cells are shown as representative.
doi:10.1371/journal.pone.0059243.g005

the addition of ATP (1 mM) for the last 30 min, (3) without LPS or ATP for 4.5 hours, to evaluate the production pattern of IL-1β in response to LPS plus ATP. [23].

The levels of IL-6, IL-10, IL-12p70 and TNFα in the supernatants of M1 or M2 macrophage culture were measured 24 hours after LPS (100 ng/ml) stimulation.

### Chemotaxis Assay

PS-Mo chemotaxis was evaluated using a trans-well migration assay with 8-μm pore size inserts (BD Biosciences). After CX3CL1 (fractalkine; R&D systems) was added to either the bottom or top of the chamber, serum-starved PS-Mo were loaded onto the inserts which were placed into 24-well plates containing RPMI-1640 and then incubated at 37°C for 5 hours. [24] Cell migration was measured by flow cytometry as previously reported: equivalent amounts of counting beads were added to each sample and the ratios of PS-Mo to the counting beads were calculated. [25].

### Antigen Uptake Assay

The antigen uptake capacity of monocytic lineage cells was evaluated as previously described. [26] Briefly, the cells were collected and stored on ice for 10 min. PS-Mo, pluripotent cell-derived immature DCs (PS-imDCs) and pluripotent cell-derived mature DCs (PS-mDCs) ($5\times10^4$ cells) were incubated with Ovalbumin Alexa fluor 488 Conjugate (Molecular Probes) at 0.1 mg/ml at 37°C or on ice for 45 min. Ice-cold FACS buffer was added in order to stop the reaction, samples washed twice, and the fluorescence intensity analyzed by flow cytometry.

### Mixed Leukocyte Reactions

Allogeneic naïve T cells ($1\times10^5$ cells per well) were purified from umbilical cord blood mononuclear cells using naïve $CD4^+$ T cell isolation kits (Miltenyi Biotec) and then co-cultured with 40 Gy-irradiated stimulator cells (PS-Mo, PS-imDC, and PS-mDC) in 96-well round bottomed culture plates for 3–5 days. $^3$H-methylthymidine (25 uCi/ml, Moravek Biochemicals and Radiochemicals) was added to the culture medium of 10% FBS-supplemented RPMI-1640 for the last 16 hours. The cells were harvested onto a filter mat (Perkin Elmer) and the $^3$H methylthymidine uptake determined using a scintillation counter (MicroBeta TriLux, Perkin Elmer).

### Ethical Considerations

This study was approved by the Ethics Committee of Kyoto University and written informed consent was obtained from each healthy volunteer.

### Statistics

Data are presented as the mean ± S.D. and the statistical significance of the differences between cultures were evaluated by Student's *t*-test.

## Results

### Differentiation of ESCs/iPSCs into Dendritic Cells and Macrophages via Monocyte-like Cells

A $KDR^+CD34^+$ hemangioblast-like population was detected in adherent cell clusters on day 6 (steps 1,2), and around 95% of supernatant cells were $CD43^+CD45^+$ hematopoietic cells on days 13–15 (step 3; **Figure 2A**). [17] Floating cells were recovered every 3–4 days in step 4 (**Figure S1**); the majority of these cells were $CD14^+$ monocyte-like cells (**Figure 2A**). These pluripotent cell-derived monocytes (PS-Mo) were similar to peripheral blood monocytes in morphology (**Figure 2B**). PS-Mo are positive for Esterase staining which was inhibited by NaF (**Figure 2C**). The percentages of PS-Mo in floating cells were constantly about 50–90% between day 18–28 (**Figure 2D and Figure S2A**). The yield of PS-Mo per 100 mm culture dish starting with about 30 colonies was $1.3\times10^6\pm0.3\times10^6$ at each step-4 medium exchange.

To derive DCs, PS-Mo were purified by magnetic sorting, and differentiated into $CD14^-CD83^-$ immature DCs (PS-imDCs) with the step 5-1 cytokine cocktail in 5 days (**Figure 2E**). PS-imDCs were stimulated with LPS and TNFα for an additional 2 days, which further differentiated them into $CD14^-CD83^+$ mature DCs (PS-mDCs) (**Figure 2F**). The differentiation efficiency of mature DCs from PS-Mo was comparable to that from primary monocytes (7.7%±0.9% vs. 16.5%±1.0%, $p=0.20$, unpaired Student's *t*-test). PS-Mo also had the potential to differentiate into macrophages (PS-MPs) with the step 5-2 cytokine cocktail. PS-MPs are morphologically comparable to primary monocyte-derived macrophages and they express typical surface markers such as CD14 and CD68 (**Figure 2G and Figure S3A,B**).

We confirmed that PS-Mo, pluripotent cell-derived DCs (PS-DCs), and PS-MPs expressed monocytic lineage-specific genes (**Figure 2H and Figure S2B**). [22,27] Collectively, by using this protocol, sufficient numbers of monocytic cell lineage cells can be obtained from a small number of human ESCs/iPSCs.

### Functional Assays for Monocytes Derived from ESCs/iPSCs

Next, we evaluated the functional activity of pluripotent cell-derived monocytic lineage cells. PS-Mo robustly produced the pro-inflammatory cytokines IL-6 and TNFα after LPS stimulation (**Figure 3A, Figure S3C**). Secretion pattern of IL-1β from PS-Mo with two stepwise signals LPS and ATP were similar to primary monocytes (**Figure 3A, Figure S3D**). [23,28].

PS-Mo expressed CX3CR1, implying chemotactic responses to CX3CL1 (fractalkine) (**Figure 3B**). PS-Mo migration in trans-well assays increased with increasing doses of CX3CL1 in the lower compartment of the chamber (**Figure 3C**). This phenomenon was not due to chemokinesis, but chemotaxis, because CX3CL1 in the top compartment could not induce PS-Mo migration into the lower compartment of the chamber. [24] We next compared the antigen uptake ability of PS-Mo, PS-imDCs, and PS-mDCs by incubating them with Ovalbumin Alexa fluor 488 Conjugate. [26] PS-Mo had the highest ability to take up antigen and as DCs matured they lost their ability to endocytose antigens (**Figure 3D**).

### Functional Assays for DCs Derived from ESCs/iPSCs

For evaluating functions of PS-DCs, we first confirmed that patterns of expression of cell surface markers on PS-imDCs/mDCs were comparable to those on primary dendritic cells (**Figure 4A, Figure S4A**). When stimulated with LPS and TNFα, PS-DCs also produced almost comparable amounts of pro-inflammatory and anti-inflammatory cytokines (**Figure 4B, Figure S4B**).

To test the ability of PS-DCs to activate naïve T cells, we next co-cultured allogeneic naïve T cells with PS-DCs and PS-Mo. As shown in Figure 4C, PS-mDCs had the most potent capacity to stimulate allogeneic T cell proliferation and this dose-response relationship was comparable to that observed with PB-DCs (Figure S4C).